Stem Cell Reports
Article
ISSCR
OPEN ACCESS

Closing the Mitochondrial Permeability Transition Pore in hiPSC-Derived Endothelial Cells Induces Glycocalyx Formation and Functional Maturation

Gesa L. Tiemeier,[1] Gangqi Wang,[1] Sébastien J. Dumas,[2,3] Wendy M.P.J. Sol,[1] M. Cristina Avramut,[4] Tobias Karakach,[2,3] Valeria V. Orlova,[5] Cathelijne W. van den Berg,[1] Christine L. Mummery,[5] Peter Carmeliet,[2,3] Bernard M. van den Berg,[1] and Ton J. Rabelink[1,*]

[1]The Einthoven Laboratory for Vascular and Regenerative Medicine, Department of Internal Medicine, Division of Nephrology, Leiden University Medical Center, Leiden, The Netherlands
[2]Laboratory of Angiogenesis and Vascular Metabolism, Department of Oncology, KU Leuven, Leuven, Belgium
[3]Laboratory of Angiogenesis and Vascular Metabolism, Center for Cancer Biology, VIB, Leuven, Belgium
[4]Department of Cell and Chemical Biology, Section Electron Microscopy, Leiden University Medical Center, Leiden, The Netherlands
[5]Department of Anatomy and Embryology, Leiden University Medical Center, Leiden, The Netherlands
*Correspondence: a.j.rabelink@lumc.nl
https://doi.org/10.1016/j.stemcr.2019.10.005

SUMMARY

Human induced pluripotent stem cells (hiPSCs) are used to study organogenesis and model disease as well as being developed for regenerative medicine. Endothelial cells are among the many cell types differentiated from hiPSCs, but their maturation and stabilization fall short of that in adult endothelium. We examined whether shear stress alone or in combination with pericyte co-culture would induce flow alignment and maturation of hiPSC-derived endothelial cells (hiPSC-ECs) but found no effects comparable with those in primary microvascular ECs. In addition, hiPSC-ECs lacked a luminal glycocalyx, critical for vasculature homeostasis, shear stress sensing, and signaling. We noted, however, that hiPSC-ECs have dysfunctional mitochondrial permeability transition pores, resulting in reduced mitochondrial function and increased reactive oxygen species. Closure of these pores by cyclosporine A improved EC mitochondrial function but also restored the glycocalyx such that alignment to flow took place. These results indicated that mitochondrial maturation is required for proper hiPSC-EC functionality.

INTRODUCTION

The ability to generate human endothelial cells (ECs) from human induced pluripotent stem cells (hiPSCs) makes it possible to consider these cells for therapeutic applications, tissue engineering, and regeneration and for disease modeling (Hasan et al., 2014; Leuning et al., 2018; Novosel et al., 2011; Phelps and Garcia, 2010). In addition to appropriate marker expression, proper functionality is required to realize most applications. While multiple protocols have described hiPSC-EC differentiation (Li et al., 2011; Ong et al., 2019; Orlova et al., 2014; Park et al., 2010; Rufaihah et al., 2011, 2013; Wimmer et al., 2019), these ECs have not yet been able to recapitulate all features of their adult (primary) counterparts (Halaidych et al., 2018; Rosa et al., 2019; Taura et al., 2009; Zhang et al., 2017).

One key aspect of endothelial function is the ability to synthesize and maintain a glycocalyx surface layer (Broekhuizen et al., 2009; Esko and Lindahl, 2001; Reitsma et al., 2007; Weinbaum et al., 2007). In the endothelium this consists of the polysaccharides heparan sulfate, hyaluronan, and chondroitin sulfate, and the proteins that interact with them; together, they mediate most of the characteristic functional aspects of the endothelium (Quarto and Amalric, 1994; Yayon et al., 1991). For example, the heparan sulfate chains provide the specific binding motifs required for protein-receptor interaction and the formation of surface gradients of chemokines and growth factors (Rabelink et al., 2017). The surface layer also functions as a barrier to control capillary fluid filtration and is critical for endothelial shear sensing and, hence, inducing endothelial quiescence (Arisaka et al., 1995; Boels et al., 2016; Boels et al., 2017; Mulivor and Lipowsky, 2004; van den Berg et al., 2006). Glycocalyx composition is regulated by the interplay of shear sensing with subsequent downstream glycolysis inhibition, which renders glycolytic intermediates available for glucobiosynthetic pathways, such as glycocalyx synthesis (Cantelmo et al., 2016).

To assess this aspect of functionality, we examined the ability of hiPSC-ECs to respond to shear stress exposure and to express a glycocalyx surface layer, and compared their ability to adopt a shear-sensitive endothelial phenotype with human microvascular ECs (hMVECs). Since several studies have demonstrated that mitochondria are linked to cell fate determination and development (Chung et al., 2007; Facucho-Oliveira et al., 2007; Folmes et al., 2012; Hom et al., 2011; Lonergan et al., 2007; Prigione and Adjaye, 2010; Vannini et al., 2016; Xu et al., 2013; Zhang et al., 2018), we investigated the effects of closing the mitochondrial permeability transition pore (mPTP) in hiPSC-ECs. While we observed no effect of shear stress as such, in contrast to hMVECs we found that mPTP closure induced mitochondrial maturation and decreased reactive oxygen species (ROS), which restored the expression of

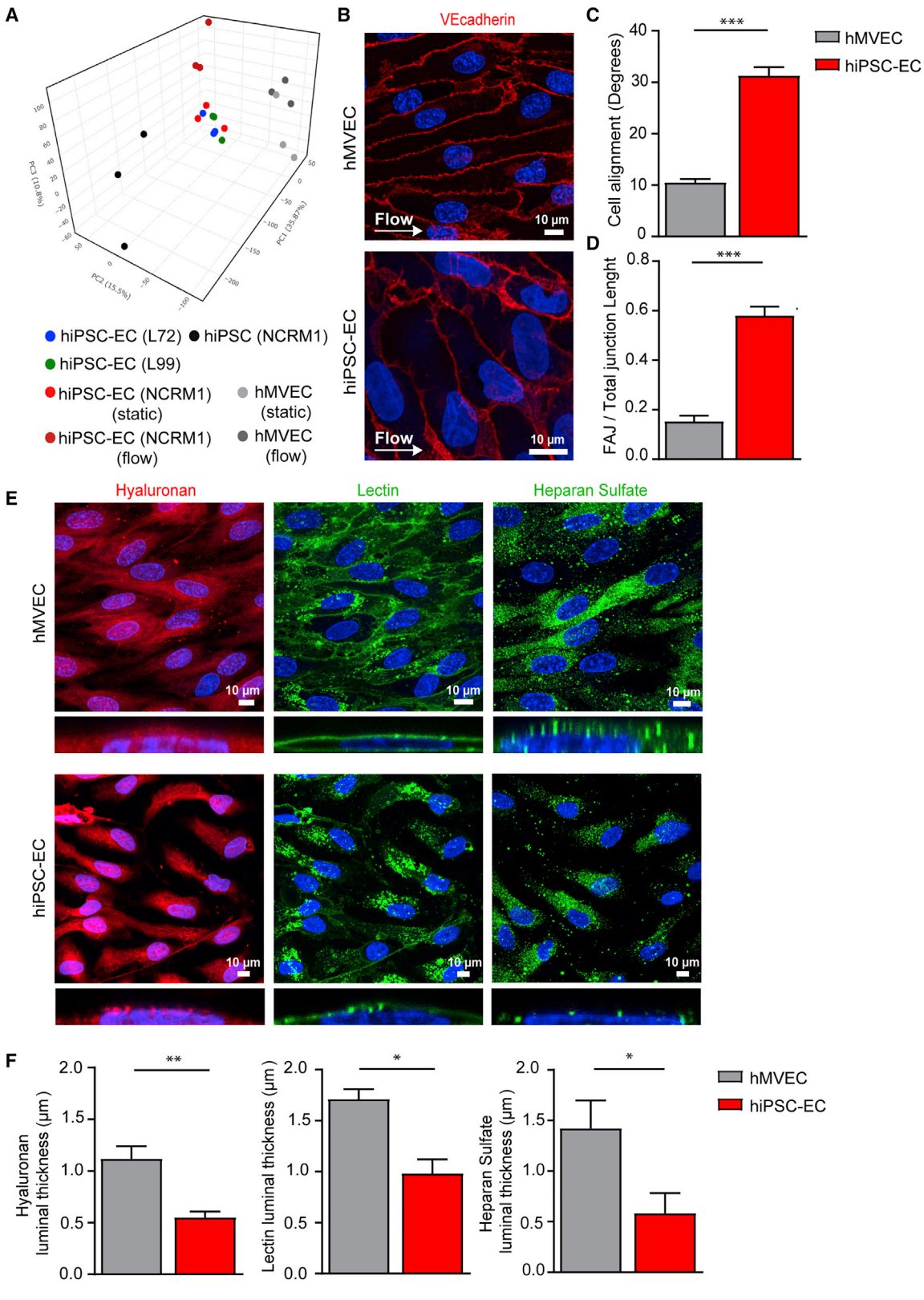

(legend on next page)

an endothelial surface layer and adaptation to shear. In this respect, hiPSC-ECs exhibited functional maturation comparable with that of hMVECs.

RESULTS

Differentiation of hiPSCs toward ECs

hiPSC lines used were generated using episomal plasmids (Okita et al., 2011) and RNA reprogramming (Schlaeger et al., 2015; Yoshioka et al., 2013) as described previously. For hiPSC-EC differentiation, we used a defined protocol described previously (Halaidych et al., 2018; Orlova et al., 2014) (Figures S1A and S1B). Results of RNA sequencing, all metabolic assays, and key experiments were obtained and reproduced in ECs from three different hiPSC lines (hiPSC-L72, hiPSC-L99, and hiPSC-NCRM1). All other results are from NCRM1 (also used as undifferentiated control). In all experiments, we compared hiPSC-ECs with primary hMVECs. For the aspects relevant to this study, we have not found significant differences between HUVECs (human umbilical vein endothelial cells) and hMVECs (Figures S2A–S2H).

Effects of Environmental Cues on iPSC-EC Functionality

To assess the effects of shear stress, we exposed hiPSC-ECs to a 5-dyne/cm^2 laminar shear stress for 4 days. Previous studies have shown that shear stress of less than 24 h provokes an inflammatory-like response and that prolonged shear stress is necessary for the assessment of response to flow, such as alignment (Dekker et al., 2002, 2006; Fledderus et al., 2007). Principal component analysis (PCA) of total RNA-sequencing data revealed that hiPSC-ECs cultured under static conditions formed a distinct population compared with hMVECs and that although flow induced a change in transcriptome, the cells were still different from the mature hMVECs (Figure 1A). Even prolonged flow had little effect on alignment of hiPSC-ECs (Figures 1B and 1C) but instead resulted in unstable focal adherence junctions between the cells (Figure 1D). Co-culturing hiPSC-ECs with human kidney-derived perivascular stromal cells for 4 days also failed to improve the alignment of hiPSC-ECs with laminar flow (Figures S3A and S3B).

hiPSC-ECs Lack a Functional Glycocalyx

As the endothelial glycocalyx serves a primary shear stress sensor (Arisaka et al., 1995; Mulivor and Lipowsky, 2004; van den Berg et al., 2006), we determined whether hiPSC-ECs had a functional glycocalyx. To this end, we quantified the luminal thickness of hyaluronan, lectin binding, and heparan sulfate (Figures 1E and 1F). Luminal glycocalyx expression was significantly lower in hiPSC-ECs compared with hMVECs with an overall ~50% decrease in thickness of hyaluronan, lectin, and heparan sulfates (Figures 1E and 1F), indicating insufficient and dysfunctional surface coverage that can be important for binding of growth factors, mechanotransduction, and vascular stability. Pericyte co-culture did not increase the luminal glycocalyx thickness either (Figures S3C and S3D).

hiPSC-ECs Have Reduced Mitochondrial Function

Since endothelial function is intrinsically linked to its metabolism (Bierhansl et al., 2017; Eelen et al., 2015), we investigated the expression of metabolic enzyme genes. PCA revealed separate clustering of undifferentiated hiPSCs, hiPSC-ECs, and hMVECs, indicating that hiPSC-ECs exhibited a different metabolic gene-expression profile with hMVECs (Figure 2A). Functional measurements of the extracellular acidification rate (ECAR), an indicator of lactate production, showed similar glucose-induced glycolysis and maximal glycolytic capacity in three different hiPSC-EC cell lines compared with hMVECs

Figure 1. hiPSC-Derived Endothelial Cells Do Not Show a Functional Response to Shear Stress Accompanied by an Insufficient Glycocalyx

(A) PCA plot of expression of all genes acquired from RNA sequencing of hiPSC NCRM1, mature ECs (hMVECs), and hiPSC-ECs NCRM1/L72/L99 in static conditions and after exposure to flow.

(B–D) Representative cross-sectional confocal images stained for VE-cadherin (red) and Hoechst (blue) after 4 days of laminar flow (5 dyne/cm^2) culture of hMVECs and hiPSC-EC NCRM1 show the alignment of cells to flow (B). Quantification of cell alignment after 4 days of laminar flow culture of hMVECs and hiPSC-ECs (100 cells/group) (C). Quantification of adherence junction remodeling as the ratio of unstable focal adherence junction (FAJ) over total adherence junction length after 4 days of laminar flow culture of hMVECs and hiPSC-ECs (50 cells/group) (D).

(E and F) Representative cross-sectional and side-view confocal images stained for components of the glycocalyx (E). Hyaluronan (Neurocan, red), lectin (LEA, green) and heparan sulfate (JM403, green) after 4 days of laminar flow (5 dyne/cm^2) culture of hMVECs and hiPSC-EC NCRM1 (E). Quantification of luminal thickness of hyaluronan, lectin *Lycopersicon esculentum*, and heparan sulfates after 4 days of laminar flow of hMVECs and hiPSC-ECs (8–16 cells/group) (F).

Values are presented as mean ± SEM of n = 3–6 independent experiments. Non-paired two-tailed Student's t test was performed; *p < 0.05, **p < 0.001, ***p < 0.0001.

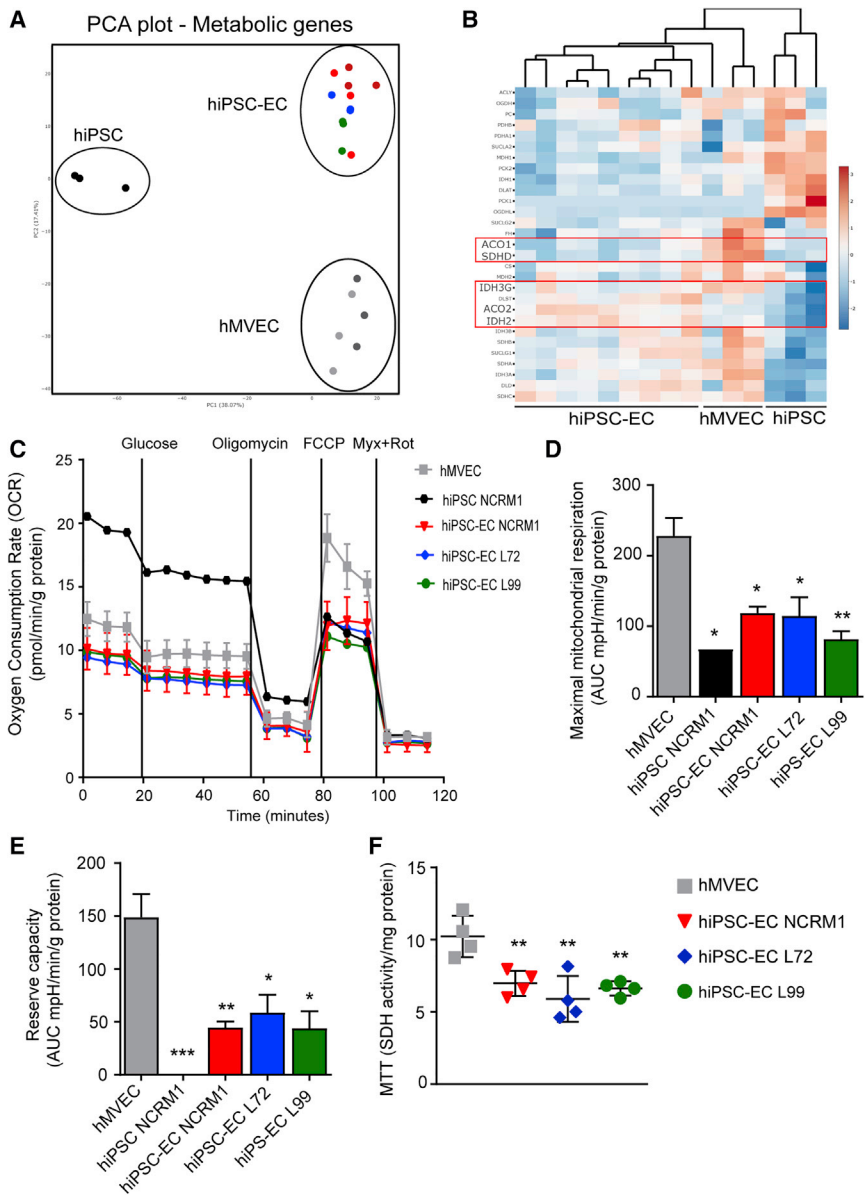

Figure 2. hiPSC-ECs Have Dysfunctional Mitochondria

(A) PCA plot of expression of all metabolic genes acquired from RNA sequencing of hiPSC NCRM1, hiPSC-ECs NCRM1/L72/L99, and mature ECs (hMVECs).

(B) Heatmap of RNA-sequencing results of metabolic genes involved in the mitochondrial metabolism. Scale bar represents *Z* scores: blue indicates lower gene expression and red a higher gene expression.

(C–E) Using a Seahorse XF flux analyzer, the oxygen consumption rate (OCR), an indicator of metabolic function, revealed mitochondrial dysfunction in three different hiPSC-EC cell lines (C). Both maximal mitochondrial respiration (D) and mitochondrial reserve capacity (E) were decreased (n = 4).

(F) Mitochondrial activity was also tested by MTT (n = 4).

Values are presented as mean ± SEM of n = 3–5 independent experiments. One-way ANOVA was performed; *p < 0.05, **p < 0.001, ***p < 0.0001.

(Figures S4A and S4B). Furthermore, ATP production was similar (Figure S4C), dismissing the lack of energy production. RNA sequencing, however, showed a clear downregulation of several enzymes related to the tricarboxylic acid cycle, including isocitrate dehydrogenase and aconitase 1 (Figure 2B). The oxygen consumption rate (OCR), an indicator of mitochondrial function, showed dysfunction in hiPSC-ECs from all three hiPSC lines (Figure 2C) (Zhang et al., 2012) demonstrated by significantly reduced maximum mitochondrial respiration and mitochondrial reserve capacity (Figures 2D and 2E). This reduced mitochondrial activity was further confirmed by reduced NAD(P)H-dependent reduction of the tetrazolium dye MTT (3-(4,5-dimethylthiazol-2-yl)-2,5-diphenyltetrazolium bromide) (Figure 2F).

hiPSC-ECs Have Immature Mitochondria

hiPSC-ECs have higher numbers of mitochondria and mitochondrial DNA compared with hMVECs (Figures 3A and 3B). However, both confocal microscopy and transmission electron microscopy (TEM) revealed a distinctly different morphology of hiPSC-EC mitochondria compared with hMVECs (Figures 3D, 3E, and S5A). TEM of the hiPSC-ECs showed round mitochondria with paucity of cristae, characteristic of immaturity. This was associated with increased cell-associated ROS (Figure 3C).

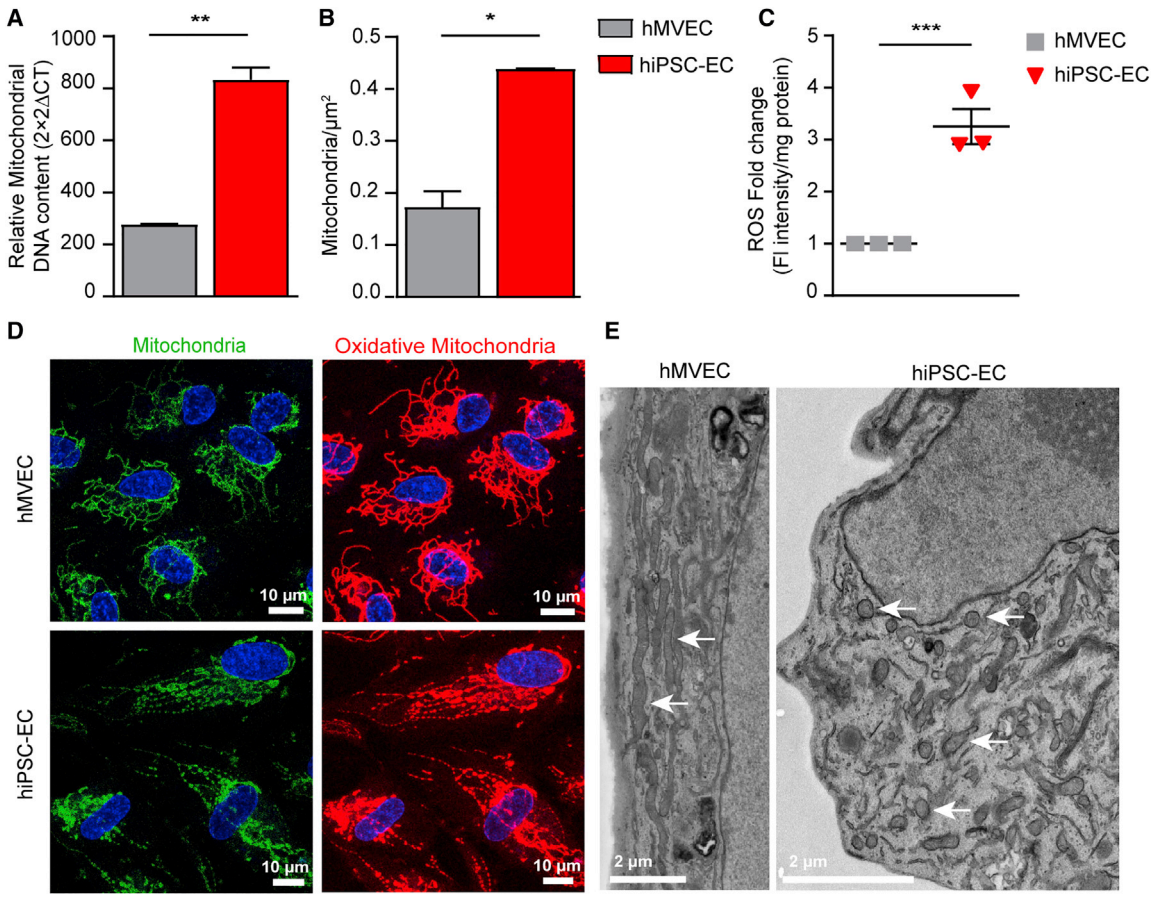

Figure 3. hiPSC-ECs Have an Increased Amount of Immature Mitochondria

(A) Mitochondrial DNA measured by qPCR.

(B) Mitochondrial density quantified on transmission electron microscopy (TEM) stitches (21 cells/group).

(C) Fold change of fluorescent intensity/mg protein of ROS dye.

(D) Representative cross-sectional confocal images stained for MitoTracker red (oxidative mitochondria) and MitoTracker green (mitochondria).

(E) TEM images show the ultrastructure of mitochondria of hMVECs and hiPSC-EC NCRM1.

Values are presented as mean ± SEM of n = 3 independent experiments. Non-paired two-tailed Student's t test was performed; *$p < 0.05$, **$p < 0.001$, ***$p < 0.0001$.

Mitochondrial Maturation by Permeability Transition Pore Closure

The high number of immature mitochondria and increased intracellular ROS in hiPSC-ECs suggested that the mitochondrial membrane permeability transition pore (mPTP) in hiPSC-ECs might be constitutively open (Halestrap, 2009; Hom et al., 2011). During differentiation of hiPSC to hiPSC-ECs, this mPTP transporter should close in order to allow maturation of the mitochondria (Hom et al., 2011). Cyclosporine A (CsA), an immunosuppressant, binds to mitochondrial cyclophilin D (CYPD) to block the calcium ion-induced permeability transition pore mPTP (Figure 4A), and treatment with CsA has been shown to induce mitochondrial maturation in myocytes (Brookes et al., 2004; Crompton et al., 1999; Halestrap, 2009; Hom et al., 2011). To determine whether the mPTP was open in hiPSC-ECs, we used the cobalt/calcein quenching method (Petronilli et al., 1999). In untreated hiPSC-ECs, calcein fluorescence leaked from the mitochondria due to an open mPTP, and calcein AM fluorescence was observed throughout the cell. However, when hiPSC-ECs were treated with 1.5 mM CsA for 30 min, only mitochondrial calcein fluorescence was observed, indicating that CsA closed the mPTP, preventing calcein leakage from the mitochondria. In untreated hMVECs, calcein fluorescence was only observed in the mitochondria, confirming the closed mPTP in mature ECs (Figures 4B and S5B).

Treatment of hiPSC-ECs with CsA for a week during differentiation starting on day 5 revealed high numbers

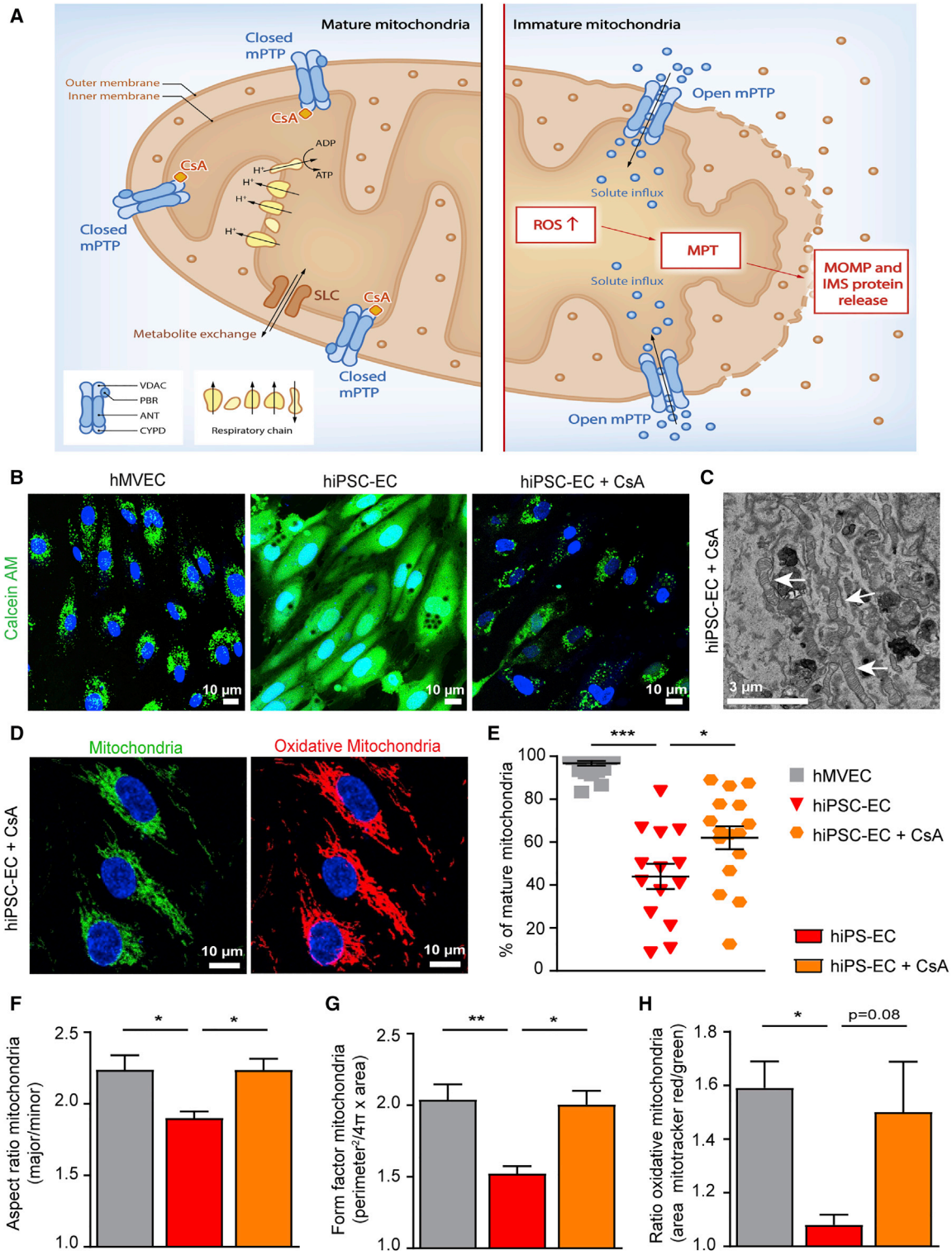

Figure 4. Treatment with Cyclosporine A Results in Closure of the mPTP and Subsequent Maturation of the Mitochondria

(A) Schematic overview of mature and immature mitochondria. Cyclosporine A (CsA) binds to cyclophilin D (CYPD) and thereby closes the mitochondrial permeability transition pore (mPTP). This prevents leakage of ROS and intermembrane space (IMS) proteins due to mitochondrial outer membrane permeabilization during the opening of mPTP.

(legend continued on next page)

of mature, elongated cristae-rich mitochondria similar to those observed in hMVECs on TEM (Figures 4C and 4E). The same morphology was observed with confocal microscopy using MitoTracker dyes (Figures 4D and S5A). Analysis of the mitochondrial morphology further supported the maturation of the mitochondria, with a higher aspect ratio and form factor in hiPSC-ECs treated with CsA, indicating increased elongation and reduced circularity of the mitochondria (Figures 4F and 4G). A trend toward more oxidative mitochondria was also observed (Figure 4H).

Improved Mitochondrial Function after Treatment with CsA

CsA treatment during the differentiation of hiPSC-ECs restored mitochondrial function by increasing maximal mitochondrial respiration and reserve capacity and increasing mitochondrial activity as detected by the MTT to levels similar to those in hMVECs (Figures 5A–5D). Concomitantly, CsA led to significantly reduced levels of ROS (Figure 4E). This reduction was also observed after treating the cells with MitoTEMPO (Figure 5E), a mitochondria-specific antioxidant, which further suggested that ROS is produced by the dysfunctional mitochondria (Figure 5E). However, treatment with MitoTEMPO during differentiation did not lead to mitochondrial maturation (Figure 5D). The reduction in ROS after treatment with CsA is not due to changes in mitochondrial content, since the amount of mitochondria is not significantly different (Figures 5F and 5G) Together, these findings indicated that maturation of mitochondria could be induced by closure of the mPTP with CsA.

Closure of mPTP Restores Glycocalyx Formation and Improves Functionality of hiPSC-ECs

After treating the hiPSC-ECs with CsA during differentiation, we exposed them to 4 days of laminar flow to assess the glycocalyx and morphological responses. The mPTP was still closed after 4 days of flow, assessed by the cobalt/calcein method as described earlier, even without addition of CsA during the flow (Figure S5C). CsA significantly increased luminal thickness of hyaluronan, lectin, and heparan sulfates compared with untreated hiPSC-ECs (Figures 6A, 6B, and S6A). Given the role of glycocalyx as a shear stress mechanotransducer, we hypothesized that normalization of the glycocalyx might lead to restoration of alignment to shear. Indeed, treatment of hiPSC-ECs with CsA resulted in improved alignment to the shear stress (Figures 6C, 6D, and S6B).

DISCUSSION

ECs exposed to laminar shear stress express a thick glycocalyx on their surface that plays an important role in reducing vascular permeability and endothelial anti-inflammatory, antithrombotic, and antiangiogenic properties. Our results show that prolonged exposure to shear stress initially failed to induce endothelial quiescence or maturation in hiPSC-ECs. We showed that hiPSC-ECs essentially lack a functional glycocalyx and do not align to the shear stress as primary ECs. Several studies have also demonstrated a role for pericytes in inducing EC quiescence and vessel stability (Lennon and Singleton, 2011; Sweeney and Foldes, 2018). Our data, however, showed that additional co-culture of hiPSC-ECs with pericytes under shear also failed to induce endothelial quiescence and the synthesis of a glycocalyx layer. Nonetheless, we recently demonstrated that pericyte-EC signaling actually requires an intact glycocalyx layer, implicating the dysfunctional glycocalyx as the potential cause for failure of hiPSC-ECs and pericyte interaction (van den Berg et al., 2019).

It has been well documented that in general, when hiPSCs commit to differentiation, they undergo metabolic remodeling so that they become less reliant on glycolysis

(B) To determine the state of the mPTP in hiPSC-ECs, the cobalt/calcein AM (green) quenching method was used. hiPSC-EC NCRM1 treated with CsA for 30 min prevented calcein leakage, indicating that CsA closed the mPTP.
(C) TEM image shows the ultrastructure of mitochondria of hiPSC-ECs treated with 500 nM CsA during differentiation.
(D) Representative cross-sectional confocal images stained for MitoTracker red (oxidative mitochondria) and MitoTracker green (mitochondria) of hiPSC-ECs NCRM1 treated with CsA. (E) Quantification of percentage of mature mitochondria on TEM stitches (21 cells/group).
(F and G) Quantitative analysis of mitochondrial morphology by analyzing MitoTracker confocal images. Individual particles (mitochondria) were analyzed for circularity and lengths of major and minor axes. From these values, aspect ratio (AR; major/minor) (F) and form factor (FF; perimeter^2/4π × area) (G) were calculated. Both FF and AR have a minimal value of 1 when a particle is a small perfect circle, and the values increase as the shape becomes elongated. AR is a measure of mitochondrial length, and an increase of FF represents increase in length and branching (10 cells/group).
(H) Quantitative analysis of the area stained by MitoTracker red (oxidative mitochondria) divided by the area stained for MitoTracker green (mitochondria) (10 cells/group).
Values are presented as mean ± SEM of n = 3–5 independent experiments. One-way ANOVA was performed; *p < 0.05, **p < 0.001, ***p < 0.0001.

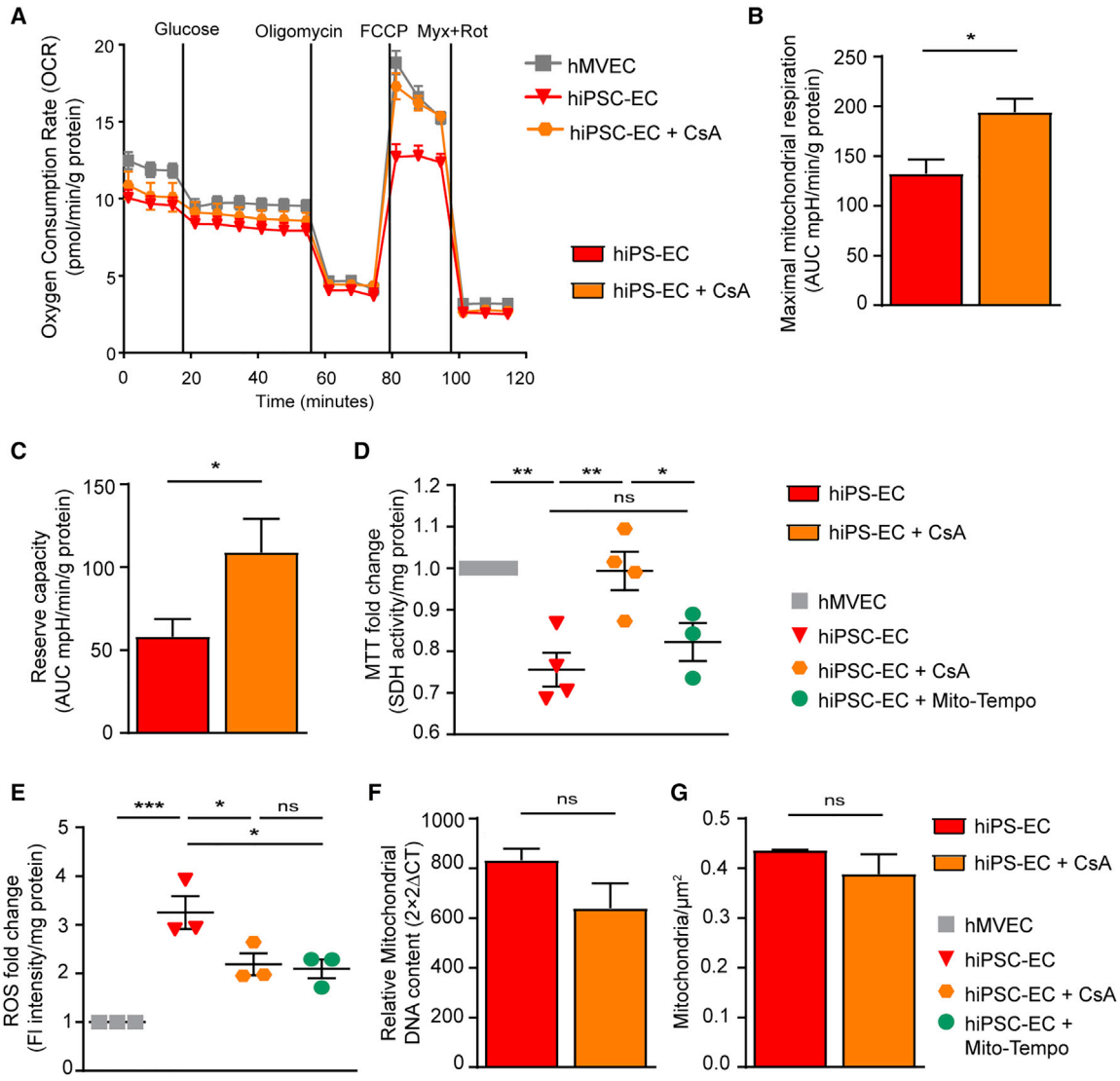

Figure 5. Treatment with Cyclosporine A Results in Improved Mitochondrial Function in hiPSC-ECs

(A–C) The OCR revealed increased mitochondrial function in hiPSC-EC NCRM1 treated with 500nM CsA during differentiation (A). Both maximal mitochondrial respiration (B) and mitochondrial reserve capacity (C) were increased in hiPSC-ECs treated with CsA (n = 3).

(D) Mitochondrial activity was also tested by MTT after addition of 500 nM CsA or 10 mM MitoTEMPO during differentiation. CsA results in an increased mitochondrial activity, whereas MitoTEMPO did not increase mitochondrial activity.

(E) Fold change of fluorescent intensity per mg of protein of ROS staining shows reduced ROS of CsA-treated cells. The same effect was obtained by addition of 10 mM MitoTEMPO.

(F and G) Mitochondrial DNA measured with qPCR (F) and mitochondrial density quantified on TEM stitches (21 cells/group) (G) after treatment of CsA during differentiation.

Values are presented as mean ± SEM of n = 3–4 independent experiments. One-way ANOVA or non-paired two-tailed Student's t test was performed; *p < 0.05, **p < 0.001, ***p < 0.0001; ns, not significant.

and more dependent upon mitochondrial respiration (Folmes et al., 2012; Xu et al., 2013; Zhang et al., 2018). This has also been described for mesodermal differentiation (Cliff et al., 2017), even though ECs preserve relatively high glycolysis (Cantelmo et al., 2016; Eelen et al., 2018; Wong et al., 2017). One hypothesis is that failure to establish an accurate metabolic switch may have negatively affected the maturation and functionality of iPSC-ECs. It was therefore noteworthy that glycolysis was not different between hiPSC-ECs and hMVECs.

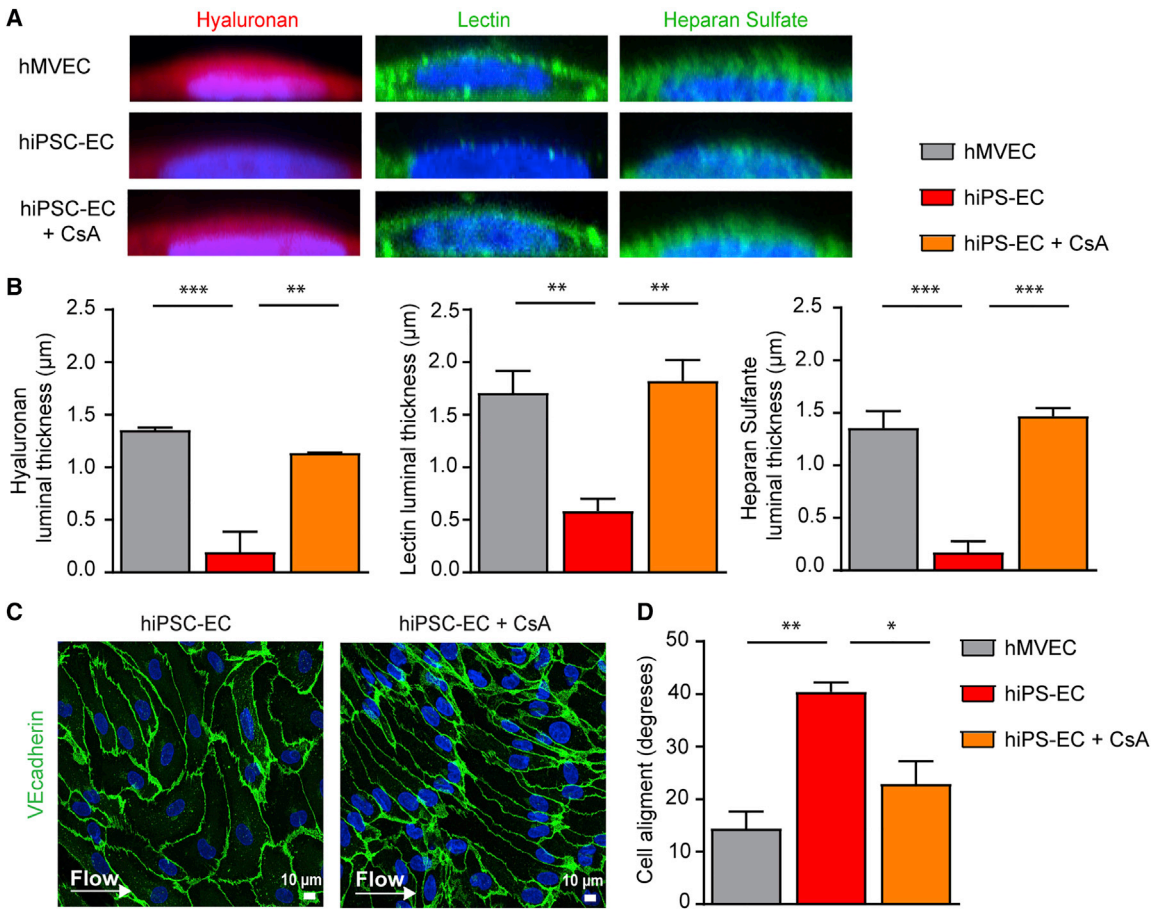

Figure 6. Treatment with Cyclosporine A Restores the Glycocalyx and Improves Alignment to Flow

(A) Representative side-view confocal images stained for hyaluronan (Neurocan, red), lectin (LEA, green), and heparan sulfate (JM403, green) after 4 days of laminar flow culture of hMVECs, hiPSC-ECs control, and hiPSC-EC NCRM1 treated with 500 nM CsA during differentiation.

(B) Quantification of luminal thickness of hyaluronan, lectin *Lycopersicon esculentum*, and heparan sulfates after 4 days of laminar flow of hMVECs, hiPSC-ECs, and hiPSC-ECs treated with CsA (8–16 cells/group).

(C) Representative cross-sectional confocal images of VE-cadherin (green) and Hoechst (blue) show the alignment of cells to flow.

(D) Quantification of cell alignment after 4 days of laminar flow culture of hMVECs, hiPSC-ECs, and hiPSC-ECs treated with CsA (100 cells/group).

Values are presented as mean ± SEM of n = 3 independent experiments. One-way ANOVA was performed; *p < 0.05, **p < 0.001, ***p < 0.0001.

The Seahorse data did show, however, reduced mitochondrial capacity for oxidative phosphorylation, despite higher overall mitochondrial content in the hiPSC-ECs. Furthermore, ultrastructural analysis showed immature, round mitochondria that lacked mature cristae development and were associated with increased ROS leakage. Together, these data indicated an open mPTP, which is characteristic of mitochondrial immaturity. Previous studies have shown the importance of mitochondria and mPTP activity in differentiation and stem cell fate (Cho et al., 2014; Hom et al., 2011; Hou et al., 2013; Wanet et al., 2015; Yan et al., 2009). Chemical closure of the mPTP has been shown to increase mitochondrial maturation, regulate redox signaling, and enhance differentiation of cardiomyocytes by 10- to 20-fold (Hom et al., 2011; Yan et al., 2009). Our data showed that prolonged closure of mPTP with CsA in hiPSC-ECs resulted in more functional mature mitochondria and prevention of ROS leakage. Furthermore, we found that maturation of the mitochondria led to functional improvements that included restoration of the glycocalyx and subsequent restoration of the mechanotransduction in hiPSC-ECs. Moreover, reduction of ROS may also be directly involved in restoration of glycocalyx, since ROS can lead to direct heparan sulfate and

hyaluronan fragmentation by oxidative reductive depolymerization (Moseley et al., 1997; Rubio-Gayosso et al., 2006; Uchiyama et al., 1990).

As ECs generate ATP mostly through glycolysis, the mitochondria act as signaling organelles via generation of ROS in addition to producing the metabolic intermediates necessary for cell growth. This activates transcriptional networks and, via metabolic intermediates, controls epigenetic regulation (Bekkering et al., 2018; Daiber et al., 2017; Kalucka et al., 2018; Schell and Rutter, 2017). The impact of mitochondrial maturation on these regulatory functions requires further study. The elongated mature mitochondria of hiPSC-ECs treated with CsA illustrate the importance of efficient biosynthetic organelles to support sufficiently the proliferation required for angiogenesis (Bruning et al., 2018; Diebold et al., 2019). This angiogenic capacity together with a functional glycocalyx, necessary for growth factor signaling and anticoagulation, is a prerequisite for future hiPSC-EC applications in tissue engineering (Leuning et al., 2018) and organoid vascularization (van den Berg et al., 2018), and in future therapeutic applications of hiPSC-ECs, such as wound healing (Clayton et al., 2018). This study demonstrated that mitochondrial maturation can be pharmacologically regulated in hiPSC-derived cells to generate more mature and representative differentiation products.

EXPERIMENTAL PROCEDURES

hiPSC Culture and EC Differentiation

NCRM1 was obtained from RUCDR (reprogramming of $CD34^+$ cord blood using episomal vectors). LUMC0072iCTRL01 (L72) and LUMC0099iCTRL04 (L99) were generated by the LUMC iPSC core facility from fibroblasts on mouse embryonic fibroblasts using a Simplicon RNA Reprogramming Kit (Millipore-Merck, Amsterdam, the Netherlands) and ReproRNA (STEMCELL Technologies) respectively, as described previously (Yoshioka et al., 2013) and further cultured in TeSR-E8 medium (STEMCELL). The hiPSC-ECs were generated from these lines according to Orlova et al. (2014). In short, hiPSCs maintained on Matrigel-coated (Corning) plates in TeSR-E8 medium were routinely enzymatically passaged weekly. Differentiation was induced 4 days after passaging (day 0). Mesoderm specification was induced by adding bone morphogenetic protein 4 (R&D Systems), activin A (Miltenyi Biotec), small-molecule inhibitor of glycogen synthase kinase 3β (Tocris Bioscience), and vascular endothelial growth factor (VEGF; Miltenyi Biotec). Mesoderm-inducing factors were removed on day 3 of differentiation and replaced by vascular specification medium containing VEGF and the transforming growth factor β (TGF-β) pathway small-molecule inhibitor SB431542 (Tocris Bioscience). SB431542 allows expansion of ECs by inhibiting the antiproliferative activities of TGF-β also present in the culture. Vascular specification medium was refreshed on days 7 and 9 of differentiation and hiPSC-ECs were isolated on day 10 using anti-CD31 antibody-coupled magnetic beads (Dynabeads; Miltenyi Biotech). hiPSC-ECs were then transferred to EC serum-free medium (EC-SFM; Gibco, Thermo Fisher Scientific) to which platelet-poor plasma (1% v/v) (Biomedical Technologies), 50 μg/mL VEGF-165 (R&D Systems), and 100 μg/mL basic fibroblast growth factor (Miltenyi Biotech) had been added (EC-SFM full medium) at 37°C with 5% CO_2 and antibiotics (100 IU/mL penicillin and 100 μg/mL streptomycin; Life Technologies Gibco).

Primary Human Microvascular EC Culture

hMVECs were isolated from human kidney cortical tissue and were purchased from Cell Systems (ACBRI-128, Kirkland, WA). They were available at passage 3 (<12 cumulative population doublings) cryopreserved in CSC Cell Freezing Medium (4Z0-705). hMVECs were also cultured in EC-SFM full medium at 37°C with 5% CO_2 and antibiotics (100 IU/mL penicillin and 100 μg/mL streptomycin).

Flow Experiments

Shear experiments were performed using an Ibidi flow system (Ibidi). Cells were cultured for 4 days at a constant laminar shear stress of 5 dyne/cm^2, at moderated physiological flow (Buchanan et al., 2014; Gautam et al., 2006) in EC-SFM full medium as previously described (Boels et al., 2016; van den Berg et al., 2019). Cells were seeded into closed perfusion chambers (ibiTreat 0.4 μ-Slide I or VI; Luer) at a concentration of 1.4×10^6 cells/mL and allowed to adhere for 3 h. Thereafter, the chamber was connected to a computer-controlled air-pressure pump and a fluidic unit with a two-way switching valve. The pump setup allowed pumping of 16 mL of cell-culture medium from two reservoirs in a unidirectional way through the flow channel over the monolayer of ECs at a constant shear stress of 5 dyne/cm^2. Medium was refreshed after 1 day of culture. The chamber and the reservoirs containing the medium were kept in an incubator at 37°C and 5% CO_2. RNA was isolated from cells subjected to shear stress in a 0.4 μ-Slide I Luer flow chamber, while the six lanes of a 0.4 μ-Slide VI Luer were used for immunofluorescent staining.

MitoTracker Staining and Quantification

MitoTracker probes (Invitrogen) were used to visualize mitochondria. Live cells were loaded with MitoTracker Green FM, MitoTracker Red CM-H2XRos (100 nM, Thermo Fisher, M7513) and Hoechst 33258 (Life Technologies, H3569) for 30 min at 37°C and imaged using a Leica SP8 white-light laser confocal immunofluorescence microscope. Analysis of mitochondrial morphology was quantified as described previously (Koopman et al., 2005; Yu et al., 2006). After filtering for median of two pixels, making the picture binary and thresholding, the individual particles were analyzed for circularity ($4\pi \times$ area/perimeter^2) and length of the minor and minor axes.

The ratio between MitoTracker red and green was also quantified by thresholding and selection of single cells, followed by measuring the stained area of MitoTracker red and MitoTracker green. For each independent experiment (n = 5), 10 cells per group were analyzed with up to 250 particles per cell.

Fluorescent Quantification

Surface hyaluronan expression (Ncan-dsRed), lectin binding (LEA; 10 μg/mL, Sigma-Aldrich, L2895) and heparan sulfate (JM403; 1.1 mg/mL, gift from Dr. van der Vlag and Dr. Kuppevelt [Nijmegen Center for Molecular Life Sciences, Radboud University Medical Center, Nijmegen, the Netherlands]) were quantified on 4 cells per field of view essentially as described earlier (Boels et al., 2016; van den Berg et al., 2019). From a side view, resliced from a line (10 pixels wide) over the nucleus, three additional lines were drawn at the nuclear position and the mean fluorescence was calculated between the distance from half-maximum signal of the nuclear staining to half-maximum signal at the luminal end. Eight to 20 cells per group were analyzed from each independent experiment (n = 4). The difference between stable adherence junctions and focal adherence junctions (FAJ) upon junction remodeling (Huveneers et al., 2012) was quantified as the ratio of FAJ length over total junction length (Timmerman et al., 2015). One hundred cells were analyzed from each independent experiment (n = 4).

Metabolic Assays

To measure endothelial glycolytic flux, we seeded hMVECs and hiPSC-ECs overnight at 4×10^4 cells per well on fibronectin-coated (Sigma-Aldrich) Seahorse XF96 polystyrene tissue culture plates (Seahorse Bioscience). The plate was incubated in unbuffered DMEM assay medium (Sigma-Aldrich) for 1 h in a non-CO_2 incubator at 37°C before measuring in an XFe 96 extracellular flux analyzer (Seahorse Bioscience). OCR (data not shown) and ECAR were measured over 4-min periods with 2-min mixing in each cycle, with five cycles in total. Inhibitors and activators were used at the following concentrations: glucose (10 mM), oligomycin (3 μM), 2-deoxyglucose (100 mM), carbonyl cyanide p-trifluoromethoxyphenylhydrazone (FCCP; 1 μM), antimycin A (1.5 μM), and rotenone (3 μM) (all Sigma-Aldrich). Cellular protein content was determined with a BCA-protein kit from Pierce (Thermo Fischer Scientific), and the data are presented as ECAR normalized to protein. Each measurement was averaged from triplicate wells. To calculate these parameters, we considered basal OCR as the last value prior to injection of the first additive (oligomycin). Likewise, we considered OCR on oligomycin as the last value prior to FCCP injection, OCR on FCCP as the last value prior to antimycin plus rotenone injection, and non-mitochondrial OCR as the last value recorded after antimycin plus rotenone.

As described previously (Dranka et al., 2010; Fink et al., 2012), we then calculated the following parameters. Basal respiration was determined as OCR in the basal state minus non-mitochondrial OCR. Maximal respiration was calculated as OCR on FCCP minus non-mitochondrial OCR. The reserve capacity was calculated as maximal respiration minus basal respiration.

To measure intracellular reactive oxygen species, we used the Cellular ROS/Superoxide detection assay kit (Abcam, ab139476). ECs plated in a black 96-well plate (20,000 cells per well) were incubated with ROS/Superoxide detection mix (2 μM) for 30 min at 37°C in darkness. As positive and negative controls, the ROS inducer pyocyanin (200 μM) and ROS inhibitor *N*-acetyl-L-cysteine (5 mM) were used 1 h or 30 min in advance, respectively. Cells were then washed twice with washing buffer and immediately observed for fluorescein and rhodamine in a Molecular Devices Spectramax i3x. Cellular protein content was determined with a BCA-protein kit from Pierce (Thermo Fisher Scientific), and the data are presented as ROS normalized to protein. Each measurement was averaged from quadruplicate wells.

CsA (Sigma, #30024) was added at a concentration of 500 nM to the vascular medium during differentiation, starting on day 5 of vascular medium, and continued for 1 week.

Statistical Analysis

Results are presented as mean ± SD or mean ± SEM, where n is the number of biological independent experimental replicates. Differences between groups were assessed by non-paired two-tailed Student's t test, paired two-tailed Student's t test, or, when not normally distributed, by two-tailed F test. Differences between more than two groups were assessed by ANOVA. p values of <0.05 were considered statistically significant.

ACCESSION NUMBERS

RNA-sequencing data are available under accession number ArrayExpress: E-MTAB-8392.

SUPPLEMENTAL INFORMATION

Supplemental Information can be found online at https://doi.org/10.1016/j.stemcr.2019.10.005.

AUTHOR CONTRIBUTIONS

G.L.T. and B.M.v.d.B. designed the research study, conducted experiments, acquired data, and wrote the manuscript. G.W., S.J.D. conducted experiments, acquired data, and provided helpful comments. M.C.A., T.K. and W.M.P.J.S conducted experiments and acquired data. C.L.M., V.V.O., and C.W.v.d.B. read the manuscript and provided helpful comments. P.C. read the manuscript, provided helpful comments, and acquired funding. T.J.R. designed the research study, wrote the manuscript, and acquired funding.

ACKNOWLEDGMENTS

We acknowledge the support of Ellen Lievers, Rozemarijn de Koning, Loes Wiersma, and Manon Zuurmond (LUMC, Leiden, the Netherlands). We thank hiPSC core facility, LUMC, Leiden, the Netherlands, for providing two hiPSC lines (LUMC0072iCTRL01 and LUMC0099iCTRL04). This work is supported by the partners of 'Regenerative Medicine Crossing Borders' (RegMed XB) and Powered by Health~Holland, Top Sector Life Sciences & Health. G.L.T. is funded by the LUMC MD/PhD track and C.W.v.d.B. is supported by the Wiyadharma fellowship (Bontius Stichting, LUMC). V.V.O. and C.L.M. received support from H2020 TECHNOBEAT.

Received: April 5, 2019
Revised: October 4, 2019
Accepted: October 5, 2019
Published: October 31, 2019

REFERENCES

Arisaka, T., Mitsumata, M., Kawasumi, M., Tohjima, T., Hirose, S., and Yoshida, Y. (1995). Effects of shear stress on glycosaminoglycan synthesis in vascular endothelial cells. Ann. N. Y Acad. Sci. *748*, 543–554.

Bekkering, S., Arts, R.J.W., Novakovic, B., Kourtzelis, I., van der Heijden, C., Li, Y., Popa, C.D., Ter Horst, R., van Tuijl, J., Netea-Maier, R.T., et al. (2018). Metabolic induction of trained immunity through the mevalonate pathway. Cell *172*, 135–146.e9.

Bierhansl, L., Conradi, L.C., Treps, L., Dewerchin, M., and Carmeliet, P. (2017). Central role of metabolism in endothelial cell function and vascular disease. Physiology *32*, 126–140.

Boels, M.G., Avramut, M.C., Koudijs, A., Dane, M.J., Lee, D.H., van der Vlag, J., Koster, A.J., van Zonneveld, A.J., van Faassen, E., Grone, H.J., et al. (2016). Atrasentan reduces albuminuria by restoring the glomerular endothelial glycocalyx barrier in diabetic nephropathy. Diabetes *65*, 2429–2439.

Boels, M.G.S., Koudijs, A., Avramut, M.C., Sol, W., Wang, G., van Oeveren-Rietdijk, A.M., van Zonneveld, A.J., de Boer, H.C., van der Vlag, J., van Kooten, C., et al. (2017). Systemic monocyte chemotactic protein-1 inhibition modifies renal macrophages and restores glomerular endothelial glycocalyx and barrier function in diabetic nephropathy. Am. J. Pathol. *187*, 2430–2440.

Broekhuizen, L.N., Mooij, H.L., Kastelein, J.J., Stroes, E.S., Vink, H., and Nieuwdorp, M. (2009). Endothelial glycocalyx as potential diagnostic and therapeutic target in cardiovascular disease. Curr. Opin. Lipidol. *20*, 57–62.

Brookes, P.S., Yoon, Y., Robotham, J.L., Anders, M.W., and Sheu, S.S. (2004). Calcium, ATP, and ROS: a mitochondrial love-hate triangle. Am. J. Physiol. Cell Physiol. *287*, C817–C833.

Bruning, U., Morales-Rodriguez, F., Kalucka, J., Goveia, J., Taverna, F., Queiroz, K.C.S., Dubois, C., Cantelmo, A.R., Chen, R., Loroch, S., et al. (2018). Impairment of angiogenesis by fatty acid synthase inhibition involves mTOR malonylation. Cell Metab. *28*, 866–880.e15.

Buchanan, C.F., Verbridge, S.S., Vlachos, P.P., and Rylander, M.N. (2014). Flow shear stress regulates endothelial barrier function and expression of angiogenic factors in a 3D microfluidic tumor vascular model. Cell Adh. Migr. *8*, 517–524.

Cantelmo, A.R., Conradi, L.-C., Brajic, A., Goveia, J., Kalucka, J., Pircher, A., Chaturvedi, P., Hol, J., Thienpont, B., Teuwen, L.-A., et al. (2016). Inhibition of the glycolytic activator PFKFB3 in endothelium induces tumor vessel normalization, impairs metastasis, and improves chemotherapy. Cancer Cell *30*, 968–985.

Cho, S.W., Park, J.-S., Heo, H.J., Park, S.-W., Song, S., Kim, I., Han, Y.-M., Yamashita, J.K., Youm, J.B., Han, J., et al. (2014). Dual modulation of the mitochondrial permeability transition pore and redox signaling synergistically promotes cardiomyocyte differentiation from pluripotent stem cells. J. Am. Heart Assoc. *3*, e000693.

Chung, S., Dzeja, P.P., Faustino, R.S., Perez-Terzic, C., Behfar, A., and Terzic, A. (2007). Mitochondrial oxidative metabolism is required for the cardiac differentiation of stem cells. Nat. Clin. Pract. Cardiovasc. Med. *4* (*Suppl 1*), S60–S67.

Clayton, Z.E., Tan, R.P., Miravet, M.M., Lennartsson, K., Cooke, J.P., Bursill, C.A., Wise, S.G., and Patel, S. (2018). Induced pluripotent stem cell-derived endothelial cells promote angiogenesis and accelerate wound closure in a murine excisional wound healing model. Biosci. Rep. *38*. https://doi.org/10.1042/BSR20180563.

Cliff, T.S., Wu, T., Boward, B.R., Yin, A., Yin, H., Glushka, J.N., Prestegaard, J.H., and Dalton, S. (2017). MYC controls human pluripotent stem cell fate decisions through regulation of metabolic flux. Cell Stem Cell *21*, 502–516.e9.

Crompton, M., Virji, S., Doyle, V., Johnson, N., and Ward, J.M. (1999). The mitochondrial permeability transition pore. Biochem. Soc. Symp. *66*, 167–179.

Daiber, A., Di Lisa, F., Oelze, M., Kroller-Schon, S., Steven, S., Schulz, E., and Munzel, T. (2017). Crosstalk of mitochondria with NADPH oxidase via reactive oxygen and nitrogen species signalling and its role for vascular function. Br. J. Pharmacol. *174*, 1670–1689.

Dekker, R., van Soest, S., Fontijn, R.D., Salamanca, S., de Groot, P.G., Vanbavel, E., Pannekoek, H., and Horrevoets, A. (2002). Prolonged fluid shear stress induces a distinct set of endothelial cell genes, most specifically lung Kruppel-like factor (KLF2). Blood *100*, 1689–1698.

Dekker, R.J., Boon, R.A., Rondaij, M.G., Kragt, A., Volger, O.L., Elderkamp, Y.W., Meijers, J.C., Voorberg, J., Pannekoek, H., and Horrevoets, A.J. (2006). KLF2 provokes a gene expression pattern that establishes functional quiescent differentiation of the endothelium. Blood *107*, 4354–4363.

Diebold, L.P., Gil, H.J., Gao, P., Martinez, C.A., Weinberg, S.E., and Chandel, N.S. (2019). Mitochondrial complex III is necessary for endothelial cell proliferation during angiogenesis. Nat. Metab. *1*, 158–171.

Dranka, B.P., Hill, B.G., and Darley-Usmar, V.M. (2010). Mitochondrial reserve capacity in endothelial cells: the impact of nitric oxide and reactive oxygen species. Free Radic. Biol. Med. *48*, 905–914.

Eelen, G., de Zeeuw, P., Simons, M., and Carmeliet, P. (2015). Endothelial cell metabolism in normal and diseased vasculature. Circ. Res. *116*, 1231–1244.

Eelen, G., de Zeeuw, P., Treps, L., Harjes, U., Wong, B.W., and Carmeliet, P. (2018). Endothelial cell metabolism. Physiol. Rev. *98*, 3–58.

Esko, J.D., and Lindahl, U. (2001). Molecular diversity of heparan sulfate. J. Clin. Invest. *108*, 169–173.

Facucho-Oliveira, J.M., Alderson, J., Spikings, E.C., Egginton, S., and St John, J.C. (2007). Mitochondrial DNA replication during differentiation of murine embryonic stem cells. J. Cell Sci. *120*, 4025–4034.

Fink, B.D., Herlein, J.A., O'Malley, Y., and Sivitz, W.I. (2012). Endothelial cell and platelet bioenergetics: effect of glucose and nutrient composition. PLoS One *7*, e39430.

Fledderus, J.O., van Thienen, J.V., Boon, R.A., Dekker, R.J., Rohlena, J., Volger, O.L., Bijnens, A.-P.J.J., Daemen, M.J.A.P., Kuiper, J., van Berkel, T.J.C., et al. (2007). Prolonged shear stress and KLF2 suppress constitutive proinflammatory transcription through inhibition of ATF2. Blood *109*, 4249.

Folmes, C.D., Dzeja, P.P., Nelson, T.J., and Terzic, A. (2012). Mitochondria in control of cell fate. Circ. Res. *110*, 526–529.

Gautam, M., Shen, Y., Thirkill, T.L., Douglas, G.C., and Barakat, A.I. (2006). Flow-activated chloride channels in vascular endothelium: shear stress sensitivity, desensitization dynamics, and physiological implications. J. Biol. Chem. *281*, 36492–36500.

Halaidych, O.V., Freund, C., van den Hil, F., Salvatori, D.C.F., Riminucci, M., Mummery, C.L., and Orlova, V.V. (2018). Inflammatory responses and barrier function of endothelial cells derived from human induced pluripotent stem cells. Stem Cell Rep. *10*, 1642–1656.

Halestrap, A.P. (2009). What is the mitochondrial permeability transition pore? J. Mol. Cell Cardiol. *46*, 821–831.

Hasan, A., Paul, A., Vrana, N.E., Zhao, X., Memic, A., Hwang, Y.S., Dokmeci, M.R., and Khademhosseini, A. (2014). Microfluidic techniques for development of 3D vascularized tissue. Biomaterials *35*, 7308–7325.

Hom, J.R., Quintanilla, R.A., Hoffman, D.L., de Mesy Bentley, K.L., Molkentin, J.D., Sheu, S.S., and Porter, G.A., Jr. (2011). The permeability transition pore controls cardiac mitochondrial maturation and myocyte differentiation. Dev. Cell *21*, 469–478.

Hou, Y., Mattson, M.P., and Cheng, A. (2013). Permeability transition pore-mediated mitochondrial superoxide flashes regulate cortical neural progenitor differentiation. PLoS One *8*, e76721.

Huveneers, S., Oldenburg, J., Spanjaard, E., van der Krogt, G., Grigoriev, I., Akhmanova, A., Rehmann, H., and de Rooij, J. (2012). Vinculin associates with endothelial VE-cadherin junctions to control force-dependent remodeling. J. Cell Biol. *196*, 641–652.

Kalucka, J., Bierhansl, L., Conchinha, N.V., Missiaen, R., Elia, I., Bruning, U., Scheinok, S., Treps, L., Cantelmo, A.R., Dubois, C., et al. (2018). Quiescent endothelial cells upregulate fatty acid beta-oxidation for vasculoprotection via redox homeostasis. Cell Metab. *28*, 881–894.e13.

Koopman, W.J., Visch, H.J., Verkaart, S., van den Heuvel, L.W., Smeitink, J.A., and Willems, P.H. (2005). Mitochondrial network complexity and pathological decrease in complex I activity are tightly correlated in isolated human complex I deficiency. Am. J. Physiol. Cell Physiol. *289*, C881–C890.

Lennon, F.E., and Singleton, P.A. (2011). Hyaluronan regulation of vascular integrity. Am. J. Cardiovasc. Dis. *1*, 200–213.

Leuning, D.G., Witjas, F.M.R., Maanaoui, M., de Graaf, A.M.A., Lievers, E., Geuens, T., Avramut, C.M., Wiersma, L.E., van den Berg, C.W., Sol, W., et al. (2018). Vascular bioengineering of scaffolds derived from human discarded transplant kidneys using human pluripotent stem cell-derived endothelium. Am. J. Transplant. *19*, 1328–1343.

Li, Z., Hu, S., Ghosh, Z., Han, Z., and Wu, J.C. (2011). Functional characterization and expression profiling of human induced pluripotent stem cell- and embryonic stem cell-derived endothelial cells. Stem Cells Dev. *20*, 1701–1710.

Lonergan, T., Bavister, B., and Brenner, C. (2007). Mitochondria in stem cells. Mitochondrion *7*, 289–296.

Moseley, R., Waddington, R.J., and Embery, G. (1997). Degradation of glycosaminoglycans by reactive oxygen species derived from stimulated polymorphonuclear leukocytes. Biochim. Biophys. Acta *1362*, 221–231.

Mulivor, A.W., and Lipowsky, H.H. (2004). Inflammation- and ischemia-induced shedding of venular glycocalyx. Am. J. Physiol. Heart Circ. Physiol. *286*, H1672–H1680.

Novosel, E.C., Kleinhans, C., and Kluger, P.J. (2011). Vascularization is the key challenge in tissue engineering. Adv. Drug Deliv. Rev. *63*, 300–311.

Okita, K., Matsumura, Y., Sato, Y., Okada, A., Morizane, A., Okamoto, S., Hong, H., Nakagawa, M., Tanabe, K., Tezuka, K., et al. (2011). A more efficient method to generate integration-free human iPS cells. Nat. Methods *8*, 409–412.

Ong, S.B., Lee, W.H., Shao, N.Y., Ismail, N.I., Katwadi, K., Lim, M.M., Kwek, X.Y., Michel, N.A., Li, J., Newson, J., et al. (2019). Calpain inhibition restores autophagy and prevents mitochondrial fragmentation in a human iPSC model of diabetic endotheliopathy. Stem Cell Reports *12*, 597–610.

Orlova, V.V., van den Hil, F.E., Petrus-Reurer, S., Drabsch, Y., Ten Dijke, P., and Mummery, C.L. (2014). Generation, expansion and functional analysis of endothelial cells and pericytes derived from human pluripotent stem cells. Nat. Protoc. *9*, 1514–1531.

Park, S.W., Jun Koh, Y., Jeon, J., Cho, Y.H., Jang, M.J., Kang, Y., Kim, M.J., Choi, C., Sook Cho, Y., Chung, H.M., et al. (2010). Efficient differentiation of human pluripotent stem cells into functional $CD34^+$ progenitor cells by combined modulation of the MEK/ERK and BMP4 signaling pathways. Blood *116*, 5762–5772.

Petronilli, V., Miotto, G., Canton, M., Brini, M., Colonna, R., Bernardi, P., and Di Lisa, F. (1999). Transient and long-lasting openings of the mitochondrial permeability transition pore can be monitored directly in intact cells by changes in mitochondrial calcein fluorescence. Biophysical J. *76*, 725–734.

Phelps, E.A., and Garcia, A.J. (2010). Engineering more than a cell: vascularization strategies in tissue engineering. Curr. Opin. Biotechnol. *21*, 704–709.

Prigione, A., and Adjaye, J. (2010). Modulation of mitochondrial biogenesis and bioenergetic metabolism upon in vitro and in vivo differentiation of human ES and iPS cells. Int. J. Dev. Biol. *54*, 1729–1741.

Quarto, N., and Amalric, F. (1994). Heparan sulfate proteoglycans as transducers of FGF-2 signalling. J. Cell Sci. *107* (Pt 11), 3201–3212.

Rabelink, T.J., van den Berg, B.M., Garsen, M., Wang, G., Elkin, M., and van der Vlag, J. (2017). Heparanase: roles in cell survival, extracellular matrix remodelling and the development of kidney disease. Nat. Rev. Nephrol. *13*, 201–212.

Reitsma, S., Slaaf, D.W., Vink, H., van Zandvoort, M.A.M.J., and Oude Egbrink, M.G.A. (2007). The endothelial glycocalyx: composition, functions, and visualization. Pflugers Arch. *454*, 345–359.

Rosa, S., Praça, C., Pitrez, P.R., Gouveia, P.J., Aranguren, X.L., Ricotti, L., and Ferreira, L.S. (2019). Functional characterization of iPSC-derived arterial- and venous-like endothelial cells. Sci. Rep. *9*, 3826.

Rubio-Gayosso, I., Platts, S.H., and Duling, B.R. (2006). Reactive oxygen species mediate modification of glycocalyx during ischemia-reperfusion injury. Am. J. Physiol. Heart Circ. Physiol. *290*, H2247–H2256.

Rufaihah, A.J., Huang, N.F., Jame, S., Lee, J.C., Nguyen, H.N., Byers, B., De, A., Okogbaa, J., Rollins, M., Reijo-Pera, R., et al. (2011). Endothelial cells derived from human iPSCS increase capillary density and improve perfusion in a mouse model of peripheral arterial disease. Arterioscler. Thromb. Vasc. Biol. *31*, e72–79.

Rufaihah, A.J., Huang, N.F., Kim, J., Herold, J., Volz, K.S., Park, T.S., Lee, J.C., Zambidis, E.T., Reijo-Pera, R., and Cooke, J.P. (2013). Human induced pluripotent stem cell-derived endothelial cells exhibit functional heterogeneity. Am. J. Translational Res. *5*, 21–35.

Schell, J.C., and Rutter, J. (2017). Mitochondria link metabolism and epigenetics in haematopoiesis. Nat. Cell Biol. *19*, 589–591.

Schlaeger, T.M., Daheron, L., Brickler, T.R., Entwisle, S., Chan, K., Cianci, A., DeVine, A., Ettenger, A., Fitzgerald, K., Godfrey, M., et al. (2015). A comparison of non-integrating reprogramming methods. Nat. Biotechnol. *33*, 58–63.

Sweeney, M., and Foldes, G. (2018). It takes two: endothelial-perivascular cell cross-talk in vascular development and disease. Front. Cardiovasc. Med. *5*, 154.

Taura, D., Sone, M., Homma, K., Oyamada, N., Takahashi, K., Tamura, N., Yamanaka, S., and Nakao, K. (2009). Induction and isolation of vascular cells from human induced pluripotent stem cells—brief report. Arterioscler. Thromb. Vasc. Biol. *29*, 1100–1103.

Timmerman, I., Heemskerk, N., Kroon, J., Schaefer, A., van Rijssel, J., Hoogenboezem, M., van Unen, J., Goedhart, J., Gadella, T.W., Jr., Yin, T., et al. (2015). A local VE-cadherin and Trio-based signaling complex stabilizes endothelial junctions through Rac1. J. Cell Sci. *128*, 3041–3054.

Uchiyama, H., Dobashi, Y., Ohkouchi, K., and Nagasawa, K. (1990). Chemical change involved in the oxidative reductive depolymerization of hyaluronic acid. J. Biol. Chem. *265*, 7753–7759.

van den Berg, B.M., Spaan, J.A., Rolf, T.M., and Vink, H. (2006). Atherogenic region and diet diminish glycocalyx dimension and increase intima-to-media ratios at murine carotid artery bifurcation. Am. J. Physiol. Heart Circ. Physiol. *290*, H915–H920.

van den Berg, C.W., Ritsma, L., Avramut, M.C., Wiersma, L.E., van den Berg, B.M., Leuning, D.G., Lievers, E., Koning, M., Vanslambrouck, J.M., Koster, A.J., et al. (2018). Renal subcapsular transplantation of PSC-derived kidney organoids induces neo-vasculogenesis and significant glomerular and tubular maturation in vivo. Stem Cell Reports *10*, 751–765.

van den Berg, B.M., Wang, G., Boels, M.G.S., Avramut, M.C., Jansen, E., Sol, W.M.P.J., Lebrin, F., van Zonneveld, A.J., de Koning, E.J.P., et al. (2019). Glomerular function and structural integrity depend on hyaluronan synthesis by glomerular endothelium. J. Am. Soc. Nephrol. *30*, 1886–1897.

Vannini, N., Girotra, M., Naveiras, O., Nikitin, G., Campos, V., Giger, S., Roch, A., Auwerx, J., and Lutolf, M.P. (2016). Specification of haematopoietic stem cell fate via modulation of mitochondrial activity. Nat. Commun. *7*, 13125.

Wanet, A., Arnould, T., Najimi, M., and Renard, P. (2015). Connecting mitochondria, metabolism, and stem cell fate. Stem Cells Dev. *24*, 1957–1971.

Weinbaum, S., Tarbell, J.M., and Damiano, E.R. (2007). The structure and function of the endothelial glycocalyx layer. Annu. Rev. Biomed. Eng. *9*, 121–167.

Wimmer, R.A., Leopoldi, A., Aichinger, M., Wick, N., Hantusch, B., Novatchkova, M., Taubenschmid, J., Hammerle, M., Esk, C., Bagley, J.A., et al. (2019). Human blood vessel organoids as a model of diabetic vasculopathy. Nature *565*, 505–510.

Wong, B.W., Marsch, E., Treps, L., Baes, M., and Carmeliet, P. (2017). Endothelial cell metabolism in health and disease: impact of hypoxia. EMBO J. *36*, 2187–2203.

Xu, X., Duan, S., Yi, F., Ocampo, A., Liu, G.-H., and Izpisua Belmonte, J.C. (2013). Mitochondrial regulation in pluripotent stem cells. Cell Metab. *18*, 325–332.

Yan, P., Nagasawa, A., Uosaki, H., Sugimoto, A., Yamamizu, K., Teranishi, M., Matsuda, H., Matsuoka, S., Ikeda, T., Komeda, M., et al. (2009). Cyclosporin-A potently induces highly cardiogenic progenitors from embryonic stem cells. Biochem. Biophysical Res. Commun. *379*, 115–120.

Yayon, A., Klagsbrun, M., Esko, J.D., Leder, P., and Ornitz, D.M. (1991). Cell surface, heparin-like molecules are required for binding of basic fibroblast growth factor to its high affinity receptor. Cell *64*, 841–848.

Yoshioka, N., Gros, E., Li, H.R., Kumar, S., Deacon, D.C., Maron, C., Muotri, A.R., Chi, N.C., Fu, X.D., Yu, B.D., et al. (2013). Efficient generation of human iPSCs by a synthetic self-replicative RNA. Cell Stem Cell *13*, 246–254.

Yu, T., Robotham, J.L., and Yoon, Y. (2006). Increased production of reactive oxygen species in hyperglycemic conditions requires dynamic change of mitochondrial morphology. Proc. Natl. Acad. Sci. U S A *103*, 2653–2658.

Zhang, J., Nuebel, E., Wisidagama, D.R., Setoguchi, K., Hong, J.S., Van Horn, C.M., Imam, S.S., Vergnes, L., Malone, C.S., Koehler, C.M., et al. (2012). Measuring energy metabolism in cultured cells, including human pluripotent stem cells and differentiated cells. Nat. Protoc. *7*, 1068–1085.

Zhang, J., Chu, L.F., Hou, Z., Schwartz, M.P., Hacker, T., Vickerman, V., Swanson, S., Leng, N., Nguyen, B.K., Elwell, A., et al. (2017). Functional characterization of human pluripotent stem cell-derived arterial endothelial cells. Proc. Natl. Acad. Sci. U S A *114*, e6072–e6078.

Zhang, H., Menzies, K.J., and Auwerx, J. (2018). The role of mitochondria in stem cell fate and aging. Development *145*. https://doi.org/10.1242/dev.143420.

Stem Cell Reports, Volume *13*

Supplemental Information

Closing the Mitochondrial Permeability Transition Pore in hiPSC-Derived Endothelial Cells Induces Glycocalyx Formation and Functional Maturation

Gesa L. Tiemeier, Gangqi Wang, Sébastien J. Dumas, Wendy M.P.J. Sol, M. Cristina Avramut, Tobias Karakach, Valeria V. Orlova, Cathelijne W. van den Berg, Christine L. Mummery, Peter Carmeliet, Bernard M. van den Berg, and Ton J. Rabelink

Supplemental Information

Supplemental data

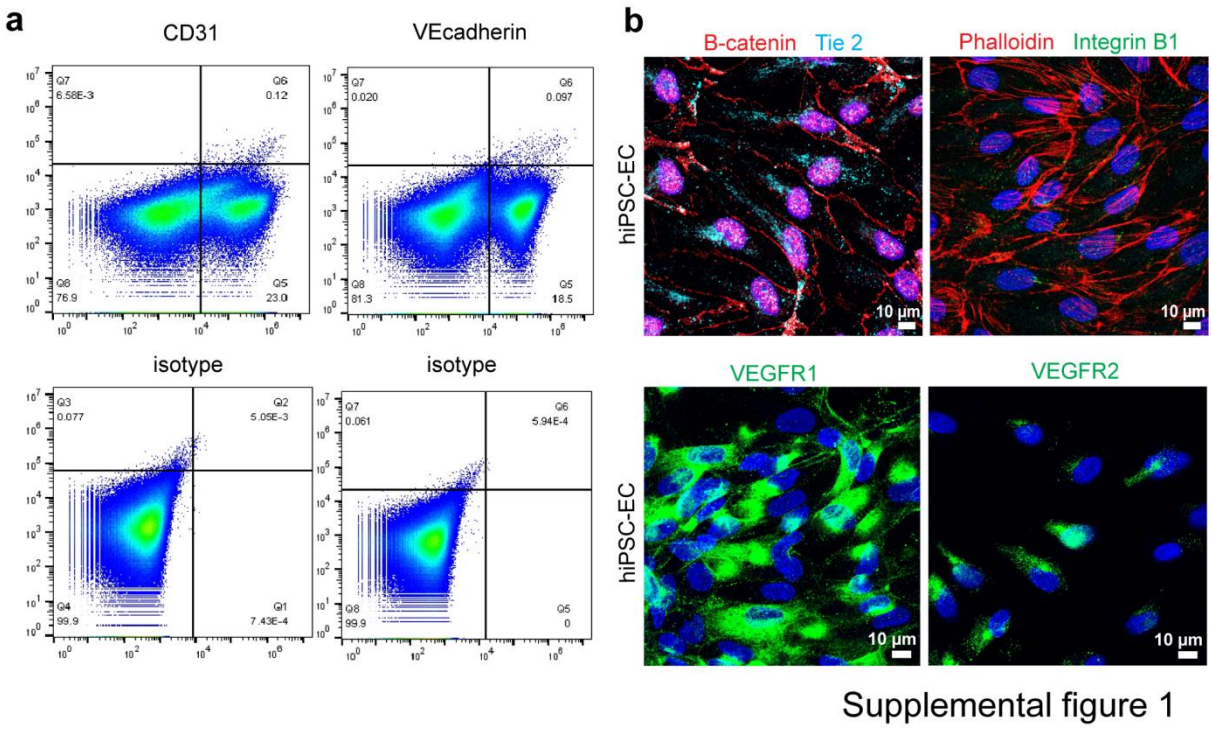

S1. **Characterization of hiPSC-ECs. Related to figure 1.**

(a) FACS analysis of cells after differentiation before CD31 bead selection shows a distinct ECs population positive for CD31 (23%) and VEcadherin (18.5%). **(b)** Representative cross-sectional confocal images stained for Tie-2 (cyan), B-catenin (red) upper left, Phalloidin (red), Integrin (green) upper right, VEGFR1 (green) lower left, VEGFR2 (green) lower right of hiPSC-ECs NCRM1.

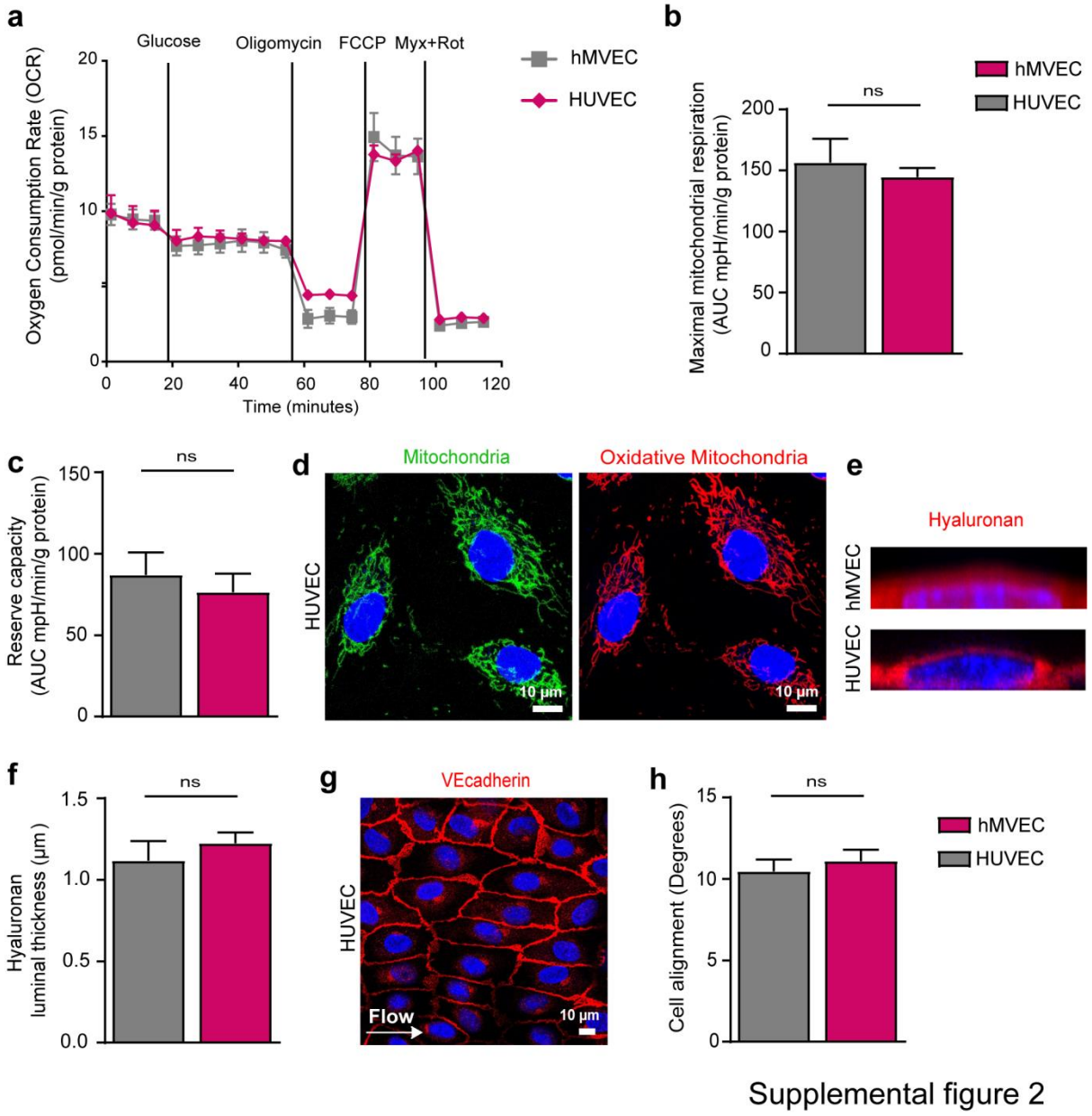

Supplemental figure 2

S2. **Comparison of hMVECs with HUVECs. Related to figure 1.**

Using a Seahorse XF flux analyzer **(a)** the oxygen consumption rate revealed no difference in mitochondrial function between hMVECs and HUVECs. Both **(b)** maximal mitochondrial respiration and **(c)** mitochondrial reserve capacity were not significantly different. **(d)** Representative cross-sectional confocal images stained for Mitotracker Red (oxidative mitochondria) and Mitotracker Green (mitochondria) of HUVECs. **(e)** Representative side view confocal images stained for Hyaluronan (Neurocan, red) after 4 days of laminar flow culture of hMVECs and HUVECs **(f)** Quantification of luminal thickness of Hyaluronan after 4 days of laminar flow of hMVECs and HUVECs. (12-20 cells/group) indicating similar glycocalyx thickness. **(g)** Representative cross sectional confocal images of VEcadherin (green) and Hoechst (blue) show the alignment of cells to flow.

(h) Quantification of cell alignment after 4 days of laminar flow culture of hMVECs and HUVECs shows similar alignment to shear stress. (100 cells/group).

Values are given as mean ± SEM of n=3-4 independent experiments. Non-paired 2-tailed Student's t-test was performed; ns = non-significant.

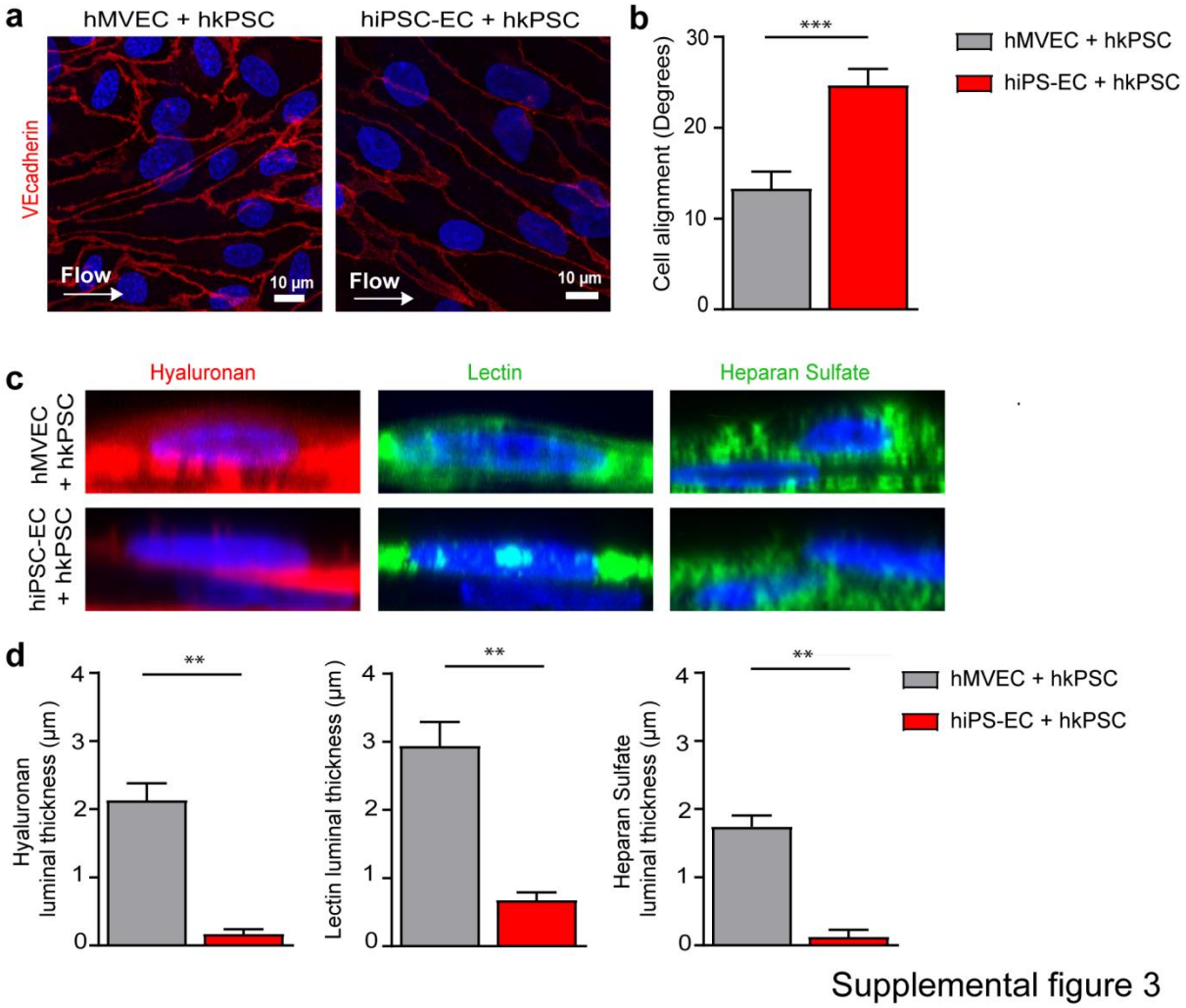

S3. **No maturation after co-culture of hiPSC-ECs NCRM1 and hMVECs with human kidney pericytes (hkPSC). Related to figure 1.**

(a) Representative cross-sectional confocal images stained VE-cadherin (red) and Hoechst (blue) after 4 days of laminar flow co-culture of hMVECs and hiPSC-ECs + hkPSC. **(b)** Quantification of cell alignment after 4 days of laminar co-culture of hMVECs and hiPSC-ECs. (100 cells/group). **(c)** Representative side view confocal images stained for Hyaluronan (Neurocan, red), Lectin (LEA, green), and Heparan Sulphate (JM403, green) after 4 days of laminar flow culture of hMVECs and hiPSC-ECs with hkPSC. **(d)** Quantification of luminal thickness of Hyaluronan, Lectin Lycopersicon esculentum, and Heparan sulfates after 4 days of laminar flow of hMVECs and hiPSC-ECs with hkPSC. (8-16 cells/group).

Values are given as mean ± SEM of n=4 independent experiments. Non-paired 2-tailed Student's t-test was performed; *P < 0.05, **P < 0.001, ***P < 0.0001.

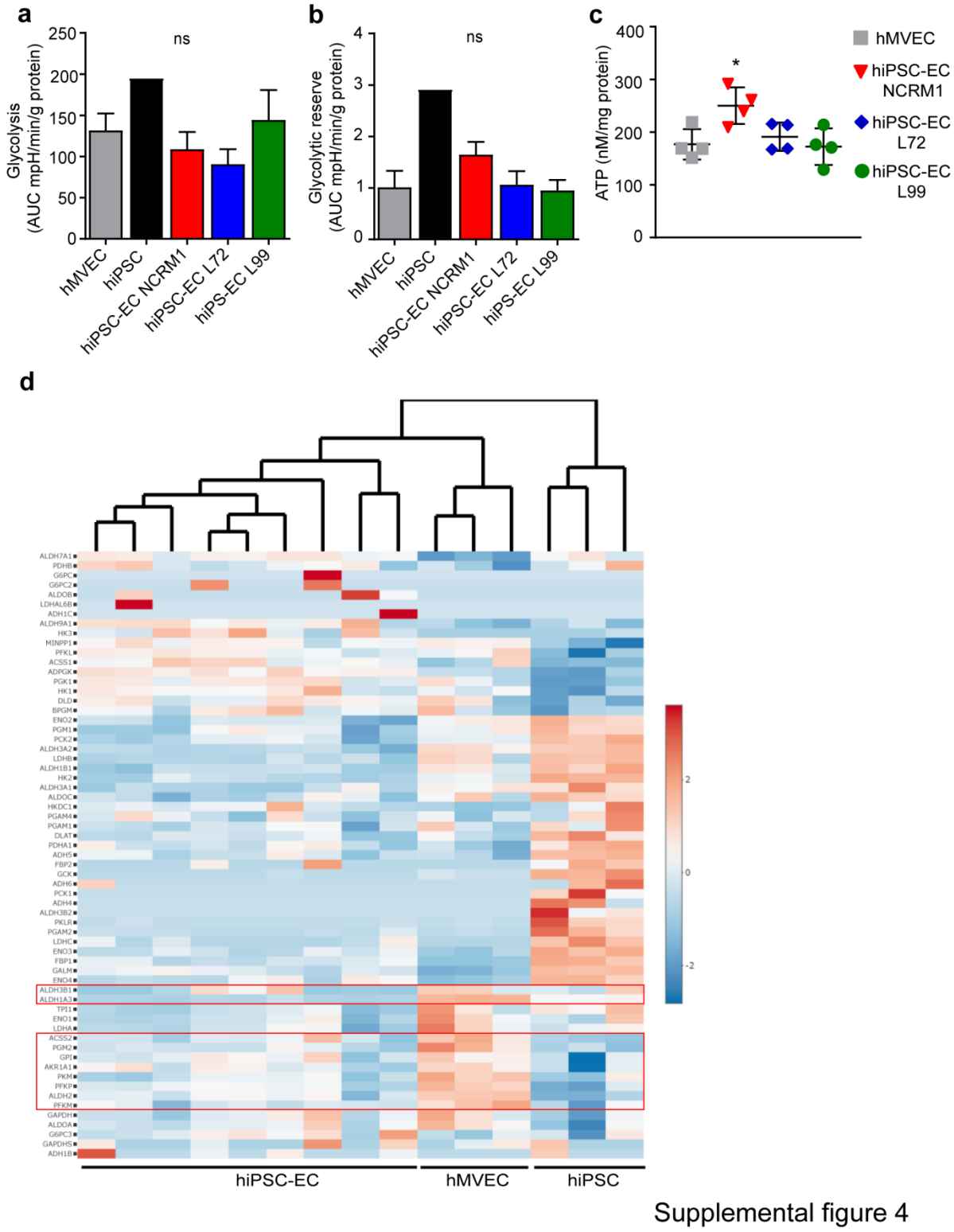

Supplemental figure 4

S4**. No functional differences in glycolysis and ATP production between hMVECs and hiPSC-ECs. Related to figure 2.**

Using a Seahorse XF flux analyzer the extracellular acidification rate (ECAR), an indicator of cellular lactate production revealed similar **(a)** glycolysis and **(b)** glycolytic reserve of tree different hiPSC-ECs cell lines and hMVECs. **(c)** ATP luciferase assay measures nM ATP per mg protein. **(d)** Heatmap of RNA sequencing results

of metabolic genes involved in the glycolysis. Scale bar represents Z-scores: blue indicates lower gene expression and red, a higher gene expression.

Values are given as mean ± SEM of n=3-4 independent experiments. one-way ANOVA was performed; *P < 0.05, **P < 0.001, ***P < 0.0001.

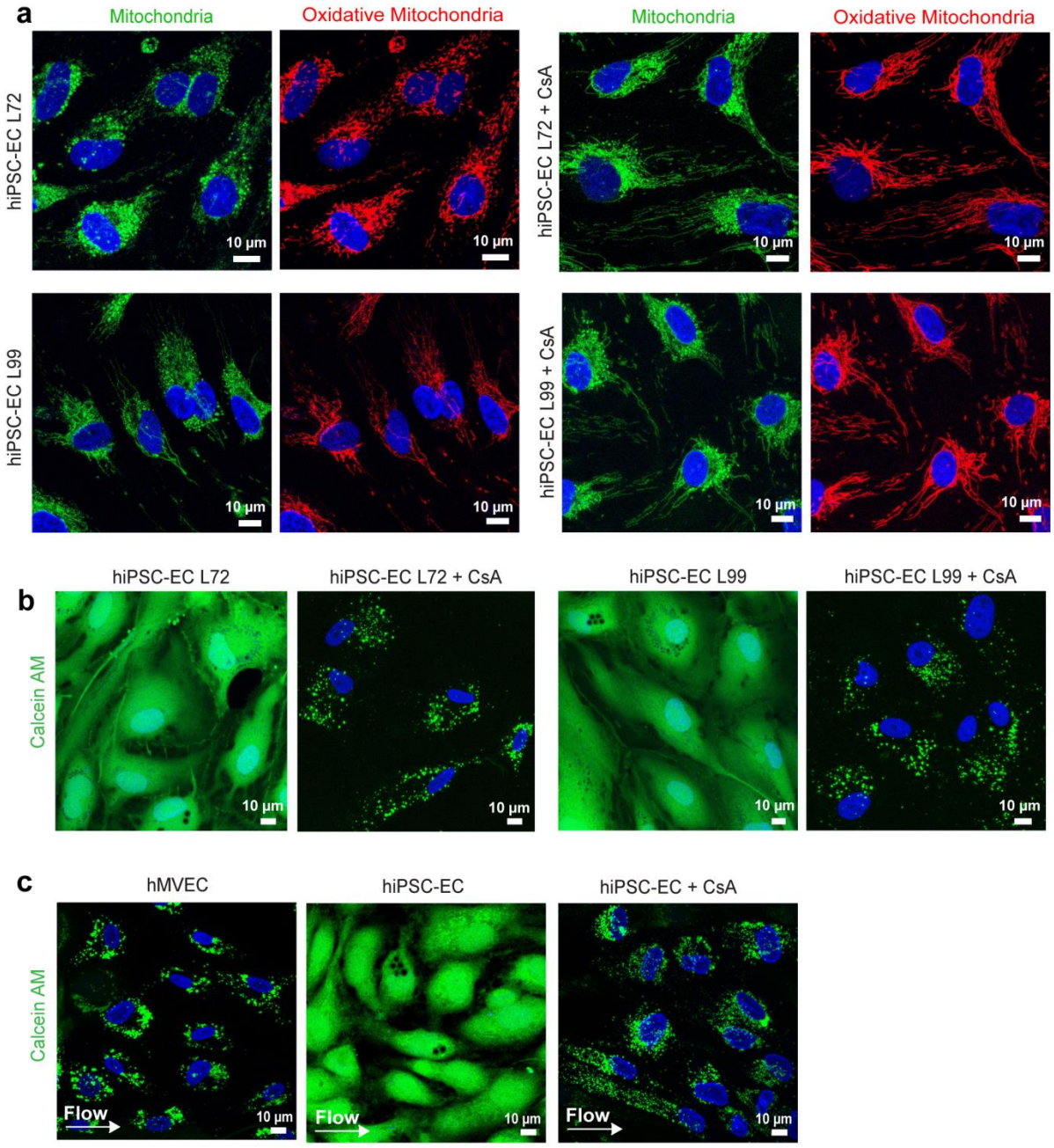

Supplemental figure 5

S5. **Treatment with cyclosporine-A results in closure of the mPTP and subsequent maturation of the mitochondria. Related to figure 4**

(a) Representative cross-sectional confocal images stained for Mitotracker Red (oxidative mitochondria) and Mitotracker Green (mitochondria) of hiPSC-ECs L72/L99 treated with CsA. **(b)** To determine the state of the mPTP in hiPSC-ECs, the cobalt/calcein AM (green) quenching method was used. hiPSC-ECs L72/L99 treated with CsA for 30 minutes prevented calcein leakage, indicating that CsA closed the mPTP. **(c)** Assessment of the state of the mPTP with Calcein AM (green) staining after 4 days flow shows prolonged effect of CsA.

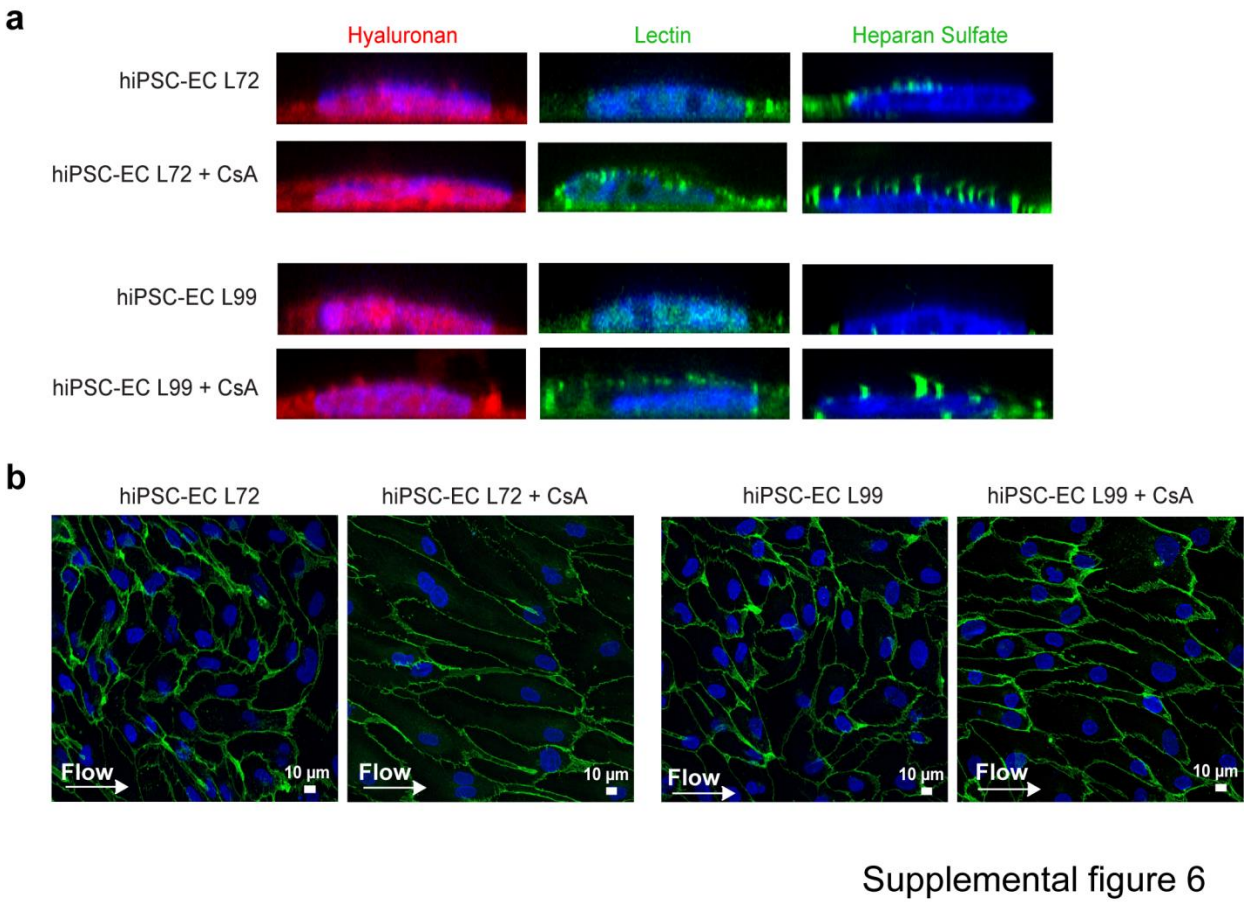

Supplemental figure 6

S6. **Treatment with cyclosporine-A restores the glycocalyx and improves alignment to flow. Related to figure 6.**

(a) Representative side view confocal images stained for Hyaluronan (Neurocan, red), Lectin (LEA, green) and Heparan Sulphate (10e4, green) after 4 days of laminar flow culture of hiPSC-ECs L72/L99 Control and hiPSC-ECs L 72/L99 treated with 500 nM CsA during differentiation. **(b)** Representative cross sectional confocal images of hiPSC-ECs L72/L99 stained for VEcadherin (green) and Hoechst (blue) show the alignment of cells to flow.

Supplemental Experimental Procedures

Primary human umbilical vein endothelial cells (HUVECs) culture

HUVECs were freshly isolated, by perfusion and subsequent incubation (20 minutes) of trypsin at 37°C, from different donors as described (Jaffe et al., 1973)(with approval of the Medical Ethical Commission of the Leiden University Medical Center, and informed consent from all subjects) and used between passage 1 and 3. Freshly isolated HUVECs were cultured on 0.5% gelatin–coated plastic flasks in endothelial basal medium medium (CCK3121; Lonza), supplemented with human epidermal growth factor, vascular endothelial growth factor, human fibroblast growth factor, R3KIGFKI, ascorbic acid, heparin, and 10% human serum (Lonza) supplemented with antibiotics (100 IU/mL penicillin and 100 μg/mL streptomycin).

Human kidney-derived perivascular stromal cells (hkPSC) culture

hkPSC were isolated from transplant grade kidneys discarded for as surgical waste (Leuning et al., 2017). In short, kidneys were perfused with collagenase (2500 units, NB1, Serva) and DNAse (2.5 mL Pulmozyme, Genentech) at 37 °C with a flow of 300mL/min via the renal artery. After approximately 30 minutes, the cell suspension was washed in DMEM-F12 (Invitrogen, Gibco) containing 10% fetal calf serum and further cultured in alphaMEM (Lonza) containing 5% platelet lysate, glutamine (Lonza) and penicillin/streptomycin and cells were cultured in tissue culture flasks until confluence was reached. At passage 1, cells were trypsinized (1X, BE02-007E, Lonza) and the $NG2^+$ cell population selected using anti-human NG2 according to manufacturer's protocol (Miltenyi Biotech).

FACS confirmed homogeneous NG2 positive hkPSC populations between passages 4-8 and hMVECs between passages 6-8, cultured in EC-SFM full medium at 37 °C and 5% CO_2.

Confocal immunofluorescence microscopy

After exposure to flow (at day 4), hMVECs and hiPSC-ECs were fixed in freshly made 4% paraformaldehyde (Alfa Aesar) in HBSS (Invitrogen, Gibco) for 10 minutes at room temperature, washed twice with HBSS /1% BSA (Sigma-Aldrich) and then blocked for 30 minutes with 3% BSA in HBSS at room temperature. 0.2% Triton (Sigma-Aldrich) was added during fixation to permeabilize the cells. Cells are incubated overnight (16 hours) at 4 °C with primary antibodies: Ncan-dsRed (1:7), VE-cadherin (1ug/mL, R&D Systems, MAB9381), JM403 (1.1mg/mL, gift from dr. van der Vlag and dr. Kuppevelt (Nijmegen Centre for Molecular Life Sciences,

Radboud University Medical Centre, Nijmegen, The Netherlands)) or the appropriate control IgG, IgG1, IgM isotype antibodies (Dako, X0931; Abcam, Ab18400) diluted in HBSS/1% BSA. After washing three times with HBSS/1% BSA, cells are incubated with Hoechst 33258 (Life Technologies, H3569), LEA FITC, Lectinfrom Lycopersicon esculentum (10 ug/mL, Sigma-Aldrich, L2895) and the appropriate secondary antibody (1:500) goat-α-mouse labeled with Alexa 488/568 (Molecular Probes, IgG1: A11001, A11004; IgG: A21121, A21124, Invitrogen, IgM: A21042) for 1 hours at room temperature. Cells were imaged using a Leica SP8 White light laser confocal immunofluorescence microscopy.

Sequential 16-bit confocal images (xyz dimensions, 0.142×0.142×0.3µm, 0.142×0.142×1µm or 0.116x0.116×1µm) were recorded using LASX Image software (Leica) and analysed with the open-source image-analysis program ImageJ (developed by W.Rasband, National Insitutes of Health, Bethesda, MD; http://rsb.info.nih.gov/ImageJ). From each independent experiment (n=4) 6-100 cells were analysed.

Detection of hyaluronan

To detect hyaluronan, a specific binding peptide from the hyaluronan binding protein neurocan conjugated to green fluorescent protein was used. Ncan-eGFP (Gift from J. Kappler) (Zhang et al., 2004) was modified in which eGFP was replaced with dsRed (Ncan-dsRed) to create a red fluorescent hyaluronan binding probe.

Transmission electron microscopy

Cell were grown in sterile cell culture dishes (PS, 35x10mm, with vents, Greiner Bio-One GmbH). Just before fixation, the medium was removed and 2.5% glutaraldehyde (Electron Microscopy Sciences)/2% paraformaldehyde (Electron Microscopy Sciences, EMS)/2mM $CaCl_2$ (Merck) in 0.15M sodium-cacodylate (Sigma-Aldrich) buffered solution was applied gently on top of the cells. Fixation was for 2 hours at room temperature. Cells were then rinsed 2x with 2mM $CaCl_2$ in 0.15 M sodium-cacodylate buffered solution, and post-fixed for 1 hour on ice with a mixture of 1% osmium tetroxide (EMS), 1.5% potassium ferrocyanide (Merck) and 2mM $CaCl_2$ in 0.15 M sodium-cacodylate buffer. Samples were further rinsed 2x with 2 mM $CaCl_2$ in 0.15M sodium-cacodylate buffer, dehydrated overnight in 70% ethanol, followed by 80% ethanol (10 min), 90% ethanol (10 min), and 100% ethanol absolute (2x 15 min; 1x30 min). The cells were then permeated with a mixture of epon LX-112 (Ladd Research) and propylene oxide (Electron Microscopy Sciences) (1:1) for 1 hour, followed by polymerization in pure epon.. Ultrathin sections (90 nm) were collected onto copper slot grids (Storck Veco) covered by Formvar film and a thin carbon layer, then stained with an aqueous solution of 7% uranyl acetate for 20 minutes, followed by Reynold's lead citrate for 10 minutes. Samples were analysed at

an acceleration voltage of 120 kV using an FEI Tecnai 12 (BioTWIN) transmission electron microscope (Thermo Fisher Scientific), equipped with a 4k Eagle CCD camera (Thermo Fisher Scientific). Automated data acquisition and stitching software was used to record virtual slides of the cells (Faas et al., 2012). Images were captured at 11.000x magnification, with binning 2, corresponding to a 2 nm pixel size at the specimen level.

Metabolic assays

To measure ATP, the Promega CellTiter-Glo reagent was used. Cells were cultured in a 96 well plate (20.000 cells per well) and the CellTiter-Glo 2.0 reagent was added 1:1 to the culture medium and mixed on an orbital shaker for 2 minutes. After 10 minutes incubation, the luminescence was recorded. A standard curve of ATP was used to quantify the total amount of ATP produced.

To determine mitochondrial activity, ECs were seeded at a density of 20.000 cells in a 24 well plate and left to adhere for 16 hours. Subsequently, cells were treated with MTT (5mg/mL, Sigma Aldrich) 1:10 in culture medium and incubated for 2 hours at 37 °C. Afterwards, MTT was removed and isopropanol/0.04M HCL added and measured at 570 nm by Molecular Devices Spectramax i3x. Cellular protein content was determined with a BCA-protein kit from Pierce (Thermo Fischer Scientific) and the data shown as MTT normalized to protein. Each measurement was averaged from triplicate wells.

RNA sequencing

RNA isolation was performed after cells in a 6-well plate reached a confluent state using a RNAeasy mini kit (Qiagen). Samples from 3 independent experiments were used for RNA sequencing. For each sample, an indexed cDNA library was prepared from 1µg total RNA using the KAPA stranded mRNA-seq kit (Sopachem). Clusters were generated using the Cbot2 system (Illumina) and amplified cDNA fragments were sequenced on a HiSeq 4000 system (Illumina) as follows: 51 cycles for read 1 and 8 cycles for index 1. The raw sequenced reads were mapped to the human reference genome build GRCh38 using STAR (Dobin et al., 2013). Mapped reads were quantified using RSEM (Li and Dewey, 2011) for accurate quantitation resulting in, on average, 34,740,890 ± 8,771,147 counts per sample. After auto-scaling, the resulting data were first summarized by principal component analysis (PCA) using the *flash*PCA (R package). Plotly was used to generate interactive graphs (2D and 3D plots). Either all genes were considered or the subset of metabolic genes present in KEGG metabolic pathways (https://www.genome.jp/kegg/) and in the Recon3D model (http://vmh.life). Heatmap analysis was performed using the *heatmaply* package. KEGG metabolic pathways were used. RNA-sequencing

data are available in ArrayExpress (https://www.ebi.ac.uk/arrayexpress/experiments/E-MTAB-8392) under accession E-MTAB-8392.

Mitochondrial DNA qPCR

DNA isolation was performed after cells reached confluence using a DNAeasy mini kit (Qiagen). qPCR for mitochondrial DNA was performed as previously described (Rooney et al., 2015). The forward and reversed mitochondrial DNA primer sequences that were used are CACCAAGAACAGGTTTGT (forward), TGGCCATGGGTATGTTGTTA (reverse). The Ct value of mtDNA is normalized by nuclear DNA, with the following sequence: TGCTGTCTCCATGTTTGATGTATCT (forward) and TCTCTGCTCCCCACCTCTAAGT (reverse).

Supplemental References

Dobin, A., Davis, C.A., Schlesinger, F., Drenkow, J., Zaleski, C., Jha, S., Batut, P., Chaisson, M., and Gingeras, T.R. (2013). STAR: ultrafast universal RNA-seq aligner. Bioinformatics (Oxford, England) *29*, 15-21.

Faas, F.G.A., Avramut, M.C., M. van den Berg, B., Mommaas, A.M., Koster, A.J., and Ravelli, R.B.G. (2012). Virtual nanoscopy: Generation of ultra-large high resolution electron microscopy maps. The Journal of cell biology *198*, 457.

Jaffe, E.A., Nachman, R.L., Becker, C.G., and Minick, C.R. (1973). Culture of human endothelial cells derived from umbilical veins. Identification by morphologic and immunologic criteria. The Journal of clinical investigation *52*, 2745-2756.

Leuning, D.G., Reinders, M.E., Li, J., Peired, A.J., Lievers, E., de Boer, H.C., Fibbe, W.E., Romagnani, P., van Kooten, C., Little, M.H., *et al.* (2017). Clinical-Grade Isolated Human Kidney Perivascular Stromal Cells as an Organotypic Cell Source for Kidney Regenerative Medicine. Stem cells translational medicine *6*, 405-418.

Li, B., and Dewey, C.N. (2011). RSEM: accurate transcript quantification from RNA-Seq data with or without a reference genome. BMC bioinformatics *12*, 323.

Rooney, J.P., Ryde, I.T., Sanders, L.H., Howlett, E.H., Colton, M.D., Germ, K.E., Mayer, G.D., Greenamyre, J.T., and Meyer, J.N. (2015). PCR based determination of mitochondrial DNA copy number in multiple species. Methods in molecular biology (Clifton, NJ) *1241*, 23-38.